Hydrolytic activity of mitochondrial F_1F_O-ATP synthase as a target for myocardial ischemia reperfusion injury: discovery, in vitro and in vivo evaluation of novel inhibitors

Panagiota-Efstathia Nikolaou[a], George Lambrinidis[b], Maria Georgiou[b], Dimitrios Karagiannis[b], Panagiotis Efentakis[a], Pavlos Bessis-Lazarou[a], Konstantina Founta[a], Stavros Kampoukos[b], Vasilis Konstantin[b], Carlos M. Palmeira[c], Sean M. Davidson[d], Nikolaos Lougiakis[b], Panagiotis Marakos[b], Nicole Pouli[b], Emmanuel Mikros[b,e*], Ioanna Andreadou[a*].

a. Laboratory of Pharmacology, Faculty of Pharmacy, National and Kapodistrian University of Athens, 15771 Athens, Greece

b. Department of Pharmaceutical Chemistry, Faculty of Pharmacy, National and Kapodistrian University of Athens, 15771 Athens, Greece.

c. Department of Life Sciences, University of Coimbra and Center for Neurosciences and Cell Biology, University of Coimbra, 3004-504 Coimbra, Portugal.

d. The Hatter Cardiovascular Institute, University College London, 67 Chenies Mews, WC1E 6HX London, United Kingdom

e. Athena Research and Innovation Center in Information Communication & Knowledge Technologies, 15125 Marousi, Greece

*I.A.: phone, +30 210 7274827, email, jandread@pharm.uoa.gr

*E.M.: phone, +302107274813; email, mikros@pharm.uoa.gr

Keywords: ATP hydrolysis, purine isosters, pyrazolopyridine, ischemia-reperfusion injury, homology modeling, induced fit docking

ABSTRACT

F_1F_O-ATP synthase is the mitochondrial complex responsible for ATP production. During myocardial ischemia, it reverses its activity hydrolyzing ATP leading to energetic deficit and cardiac injury. We aimed to discover novel inhibitors of ATP hydrolysis accessing the drugability of the target within ischemia(I)/reperfusion(R) injury. New molecular scaffolds were revealed using ligand-based virtual screening methods. Fifty-five compounds were tested on isolated murine heart mitochondria and on H9c2 cells for their inhibitory activity. A pyrazolo[3,4-*c*]pyridine hit structure was identified and was optimized in a hit-to-lead process synthesizing nine novel derivatives. Three derivatives significantly inhibited ATP hydrolysis in *vitro*, while *in vivo* they reduced myocardial infarct size (IS). The novel compound **31** was the most effective in reducing IS, validating that inhibition of F_1F_O-ATP hydrolytic activity can serve as a target for cardioprotection during ischemia. Further examination of signaling pathways revealed that the cardioprotection mechanism is related to the increased ATP content in the ischemic myocardium, increased phosphorylation of PKA and phospholamban, leading to reduction of apoptosis.

INTRODUCTION

Cardiovascular disease is a major contributor to global mortality and morbidity, and acute myocardial infarction (AMI) is the leading cause of premature deaths. Although reperfusion therapy has improved clinical outcomes and is the gold standard for the treatment of AMI, it paradoxically induces myocardial injury.[1] The ischemia/reperfusion injury (IRI) is an important risk factor for the development of heart failure and contributes to the long-term mortality (1 year and beyond) of patients surviving AMI.[2,3] Certain "cardioprotective" interventions can limit IRI and infarct size (IS)[4] following AMI, which is important, since IS is the main determinant of prognosis in AMI patients.[4,5] Several decades of systematic research on cardioprotection has revealed mechanical or pharmacological interventions that can induce cardioprotective signaling cascades.[6,7] However, most interventions and pharmacological candidates tested on AMI have failed to improve clinical outcomes or cardiac function in large clinical trials.[8,9] Thus, the identification of novel targets for therapeutic interventions is urgently needed to improve cardiovascular disease therapy.[10]

F_1F_O-ATP synthase, is the key energy generator for the majority of lifeforms on earth.[11] This large, mitochondrial multiprotein complex is embedded in the inner mitochondrial membrane along with the I-IV respiratory chain complexes and utilizes the proton motive force (PMF) in order to phosphorylate adenosine diphosphate (ADP) and produce (adenosine triphosphate) ATP[12]. ATP synthase is a mechanic rotor composed of 29 protein subunits[13] with two functionally different domains. The F_O region is embedded in the mitochondrial membrane and rotates to accept protons while the F_1 portion protrudes into the mitochondrial matrix space and is responsible for the ATP synthesis.[14] F_1F_O-ATPase hydrolyses ATP in a reverse process, inducing the reverse rotation (counterclockwise) of the central stalk and thus pumping protons across the membrane.

ATP synthase is essential for cellular viability thus is exploited (by both micro-organisms and humans) as a target to kill unwanted cells.[11,15] *Streptomyces* produce Oligomycin (*Figure 1B*), which inhibits ATP synthase by binding into the F_O domain and kills foreign organisms. It blocks both the synthesis and the hydrolysis of the ATP, and therefore it is a non-selective ATP synthase inhibitor.[16] In F_1 domain at least three cavities have been experimentally determined for small molecules binding.[17,18] The first is the catalytic center where ADP is transformed to ATP, the second is the Aurotrovertin B binding pocket in the β subunit,[13] and the third is the resveratrol binding pocket among β, α, and γ subunits (*Figure 1A*). Several inhibitors of the o-ATP synthase have been developed as antibiotics or anticancer agents[11,15] and certain polyphenolic natural products, including resveratrol and quercetin (*Figure 1B*), have been proposed as mitochondrial F_1F_O-ATP synthase inhibitors.[19]

Despite the accumulation of knowledge on the function of ATP synthase during the last decades, the effect of ATP hydrolysis inhibitors in cardiac IRI and cardioprotection has not been elucidated. During ischemia, the oxygen supply is compromised, F_1F_O-ATP synthase reverses its activity to maintain membrane potential[20] representing a subtle balance between cell life and death.[21] The first indication that ATPase may serve as a target against the ischemic insult was reported by Atwal etal.[22] In the latter report, 4-(N-arylimidazole)-substituted benzopyran derivatives were synthesized as ATP hydrolysis inhibitors and the best compound, later on named as BMS-199264,[22,23] resulted in increased time to onset of contracture in isolated rat hearts subjected to a 25-min global ischemia followed by a 30-min reperfusion. However, the mechanism of binding of BMS-199264 to ATPase as well as the mechanism of protection in the *ex vivo* hearts have not been defined and no further original publications have confirmed its cardioprotective effects. In 2008, an endogenous ATPase inhibitor selective towards the hydrolase activity was discovered. Known as “inhibitor protein of F_1 subunit” or IF_1, it is a small nuclear-encoded endogenous inhibitor of the F_1 domain of the mitochondrial F_1F_O-ATP synthase.[24] A

second small molecule inhibitor, a substituted benzoate termed BTB06584 (BTB) was designed as an ATP hydrolysis inhibitor and has been proposed to bind to IF_1 protein and alleviate ischemic injury.[21] BTB was evaluated in an *in vitro* setting of hypoxia-reoxygenation with the use of a cell line mimicking cardiomyocytes[21]. Although, this molecule was not tested on primary cells or on an *in vivo* model of IR, the selectivity of the compound towards the inhibition of ATP hydrolysis versus synthesis was encouraging.

To the best of our knowledge, there are currently no data in the literature regarding the effect of ATP hydrolysis inhibitors on IS reduction which is the gold standard measurement for cardioprotection.[25] Additionally, none of the above-mentioned small molecule inhibitors have been evaluated *in vivo,* nor the underlying mechanisms of cardioprotection deciphered using animal models of cardiac IR.

Taking the above into consideration, we aimed to discover novel inhibitors of the hydrolytic activity of F_1F_O-ATP synthase and to validate this target in the setting of cardioprotection. Our approach is illustrated in the *Supporting Information, Figure S1* and was comprised of a ligand-based *in silico* library screening to identify promising hits with initial evaluation of their potency *in vitro* on isolated murine mitochondria and on H9c2 cells followed by synthetic optimization. Then, a theoretical structure of *Mus musculus* ATP synthase was constructed based on homology modeling, and docking simulations were carried out in different binding cavities (*Figure 1A*) to understand the structural insights related to the mode of action of the most potent analogue. Finally, we sought to validate inhibition of ATP hydrolysis as a target for cardioprotection and understand its role in three particular respects: a) to identify whether inhibition of the hydrolytic activity of ATP synthase could serve as a target for cardioprotection *in vivo*, b) to examine whether the time of administration of an ATP hydrolysis inhibitor in relation to the onset of ischemia may affect the cardioprotective effect and c) to investigate the signaling downstream of ATP hydrolysis inhibition that is required for cardioprotection.

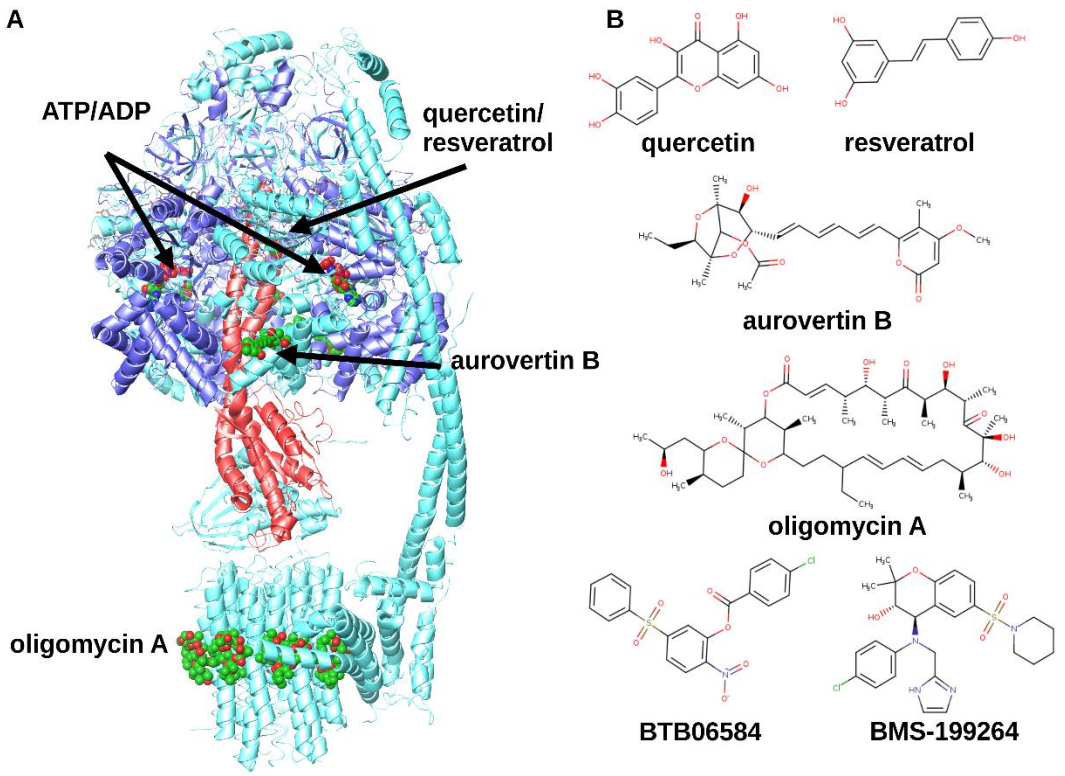

Figure 1: The mitochondrial F_1F_O ATP synthase A) *Ribbon representation of Mus musculus F_1F_O-ATP synthase. The known binding sites of ATP/ADP, Aurovertin, Quercetin/Resveratrol and Oligomycin are depicted. The γ subunit is colored red and α subunits are colored dark blue.* ***B****) Chemical structures of known non- selective F_1F_O-ATP synthase inhibitors namely quercetin, resveratrol, aurovertin B and oligomycin A and the inhibitors of the hydrolytic activity of the enzyme namely BMS-199264 and BTB06584.*

RESULTS AND DISCUSSION

Discovery of new inhibitors

a) In silico and *in vitro* studies for the identification of hit compounds.

In order to identify new molecular scaffolds targeting the F_1F_O ATP synthase hydrolytic activity we followed a ligand based *in-silico* workflow. Considering the established inhibitors BMS199264 and BTB (*Figure 1B*) a similarity search was performed using the ROCS algorithm as implemented on OpenEye software. The similarity search was conducted on our in-house library of 2000 compounds (synthetic

and natural products) named "Pharmalab",[26] and on National Cancer Institute (NCI) Open Database Compounds containing ~260,000 molecules (https://cactus.nci.nih.gov/download/nci/) *(Supporting Information, Figure S1*). Different steps of filtering through the *in-silico* screening were followed as described previously in order to select different molecular scaffolds[27] and resulted in 34 molecules from Pharmalab (*Supporting Information, Table S1*) and 15 molecules from NCI database (*Supporting Information, Table S2*).

The selected 49 hit compounds were evaluated *in vitro* on isolated murine heart mitochondria to verify their inhibitory effect on F_1F_O ATP synthase hydrolytic activity. Briefly, in this assay we excised the murine hearts which were used for isolation of mitochondria. Upon a freeze-thaw cycle of mitochondria, the mitochondrial membranes are disrupted and exposed. Due to the lack of proton gradient, the addition of ATP leads to the ATP hydrolysis and production of phosphate. At the end of the assay, the addition of the molybdate reagent leads a reaction with the phosphate which is quantified via a colorimetric assay using a single point measurement with the use of a standard curve. The % inhibition or % activity against ATP hydrolysis is calculated via the control of the assay in which DMSO, the diluent of the compounds is used as vehicle and reached the maximum activity. This assay was not performed on an isolated ATP synthase, but our experiment on isolated mitochondria, relies on the evaluation of the enzyme in fragmented mitochondrial membranes that expose the enzyme and could serve as a substitution for the isolated enzyme. The assay was performed using compounds at 200 µM which was chosen based on the fact that the previously described ATP hydrolase inhibitor BTB is effective at 100 µM.[21] Via the *in vitro* assay, it was revealed that out of the 49 hits, two compounds, namely **1124** and **202,** exhibited over 50% inhibition suggesting that these could be considered as lead compounds (*Figure 2A and Supporting Information, Table S1*). 10uM oligomycin was used as a positive control in the assay, as was resveratrol (compound **198**), which has previously been described as an inhibitor of F_1F_O-ATP synthase.[19]

Compound **1124** is a synthetic pyrazolopyridine derivative while compounds **202** and **203,** that also caused significant inhibition of the F_1F_O-ATPase's hydrolytic activity in the *in vitro* experiment, are benzofuran natural products. Their chemical structures are demonstrated in *Figures 2E* and *2G*, respectively. Since, benzofuran-bearing compounds have been already described as F_1F_O-ATP synthase inhibitors, as well as ATPases binders in different diseases contexts,[13,28,29] the pyrazolopyridine derivative **1124** was selected as the most interesting for further development. Therefore, a second round of *in silico* similarity calculations was performed against all pyrazolopyridines in Pharmalab, which resulted in the selection of additional six molecules, namely **1104**, **1110**, 1**112**, **1115**, **1117** and **1119**. These derivatives were 3-phenylsubstituted pyrazolo[3,4-*c*]pyridines, possessing also the 4-methoxybenzyl moiety at position 1 of the central pyrazolopyridine core, similarly to **1124** (except from compound **1110**). *In vitro* screening of the six new hits revealed that two more derivatives **1117** and **1119** exhibited *in vitro* improved inhibition compared to the initial hit **1124** (*Figure 2B and Supporting Information, Table S3*). Both **1117** and **1119** were substituted at position 5 with the same side chain, namely 4-(4-methylpiperazin-1-yl)aniline, suggesting that this group is favorable concerning the inhibitory activity, compared to the chlorine group of **1124** *(Figure 2G).* Several reports have delt with the identification of small molecule modulators of F_1F_O-ATP synthase which can be classified into various classes, such as polyketide, polyphenols, cationic, peptides, endogenous ligands, natural small molecules and synthetic modulators.[13] These modulators bare phenolic moieties and form hydrogen and nonpolar interaction with the ATP synthase enzyme in order to act as antimicrobial F_1F_O-ATP synthase inhibitors.[30] Via our hit to lead compound *in silico* homology-based screening, we identified for the first time that the pyrazolopyridine scaffold can interact with the mammalian F_1F_O ATP synthase.

In order to confirm the *in vitro* screening results and select lead compounds for further development, we then determined the IC_{50} values of the best candidates

using the same assay on isolated murine mitochondria. Oligomycin and resveratrol (198) (*Figure 1C*) exhibited the lowest IC_{50} values for the inhibition of ATP hydrolysis (18.5 ±1.2 μM and 65.6 ±1.2 μM, respectively) (*Figure 2D).* In this context, we also evaluated the effect of another natural product, quercetin (*Figure 2C*), which exhibited an IC_{50} value of 128.3±1.1 μM (*Figure 2D*). Resveratrol and quercetin have been shown to also inhibit the ATP synthesis[16,19] and therefore were not further examined. Additionally, in this assay we tested BTB (*Figure 2C*) which has been previously described as a selective inhibitor of ATP hydrolysis. Its effective dose at a cellular level has been determined at 100μM. With the use of our *in vitro* assay in isolated mitochondria we determined that the IC_{50} value of BTB for ATP hydrolysis is 347.2±1.1μM (*Figure 2D*). We then examined the IC_{50} values of our lead compounds. The three inhibitors sharing the pyrazolopyridine scaffold, namely **1117**, **1119** and **1124** (*Figure 2G*), displayed the lowest IC_{50} values (85.5 ±1.1 μM, 107.3 ±1.1 μM, 150.3 ±1.2μM) (*Figure 2H*). The IC_{50} values of benzofuran-based candidates, **202** and **Ebefuran III** (*Figure 2E*) were higher ranging from 161.5 to 302.8μM (*Figure 2F*). Compound **203** did not exhibit considerable inhibition since even in the highest concentration did not result in over 50% inhibition. A limitation of our method is that we could not test higher concentrations of the compounds due to their solubility in ATP assay buffer and the IC_{50} calculation of **203** is questionable. Taking these results under consideration, we proceeded to further characterize the biological activity of the three promising pyrazolopyridine compounds at a cellular level. The ATP synthase hydrolytic activity takes place in coupled intact mitochondria and is increased by respiratory chain defects[31]. A limitation of our study is that we did not examine mitochondrial respiration and also the effect of the candidates under different states of respiration as it has been described for different mitochondrial diseases[31].

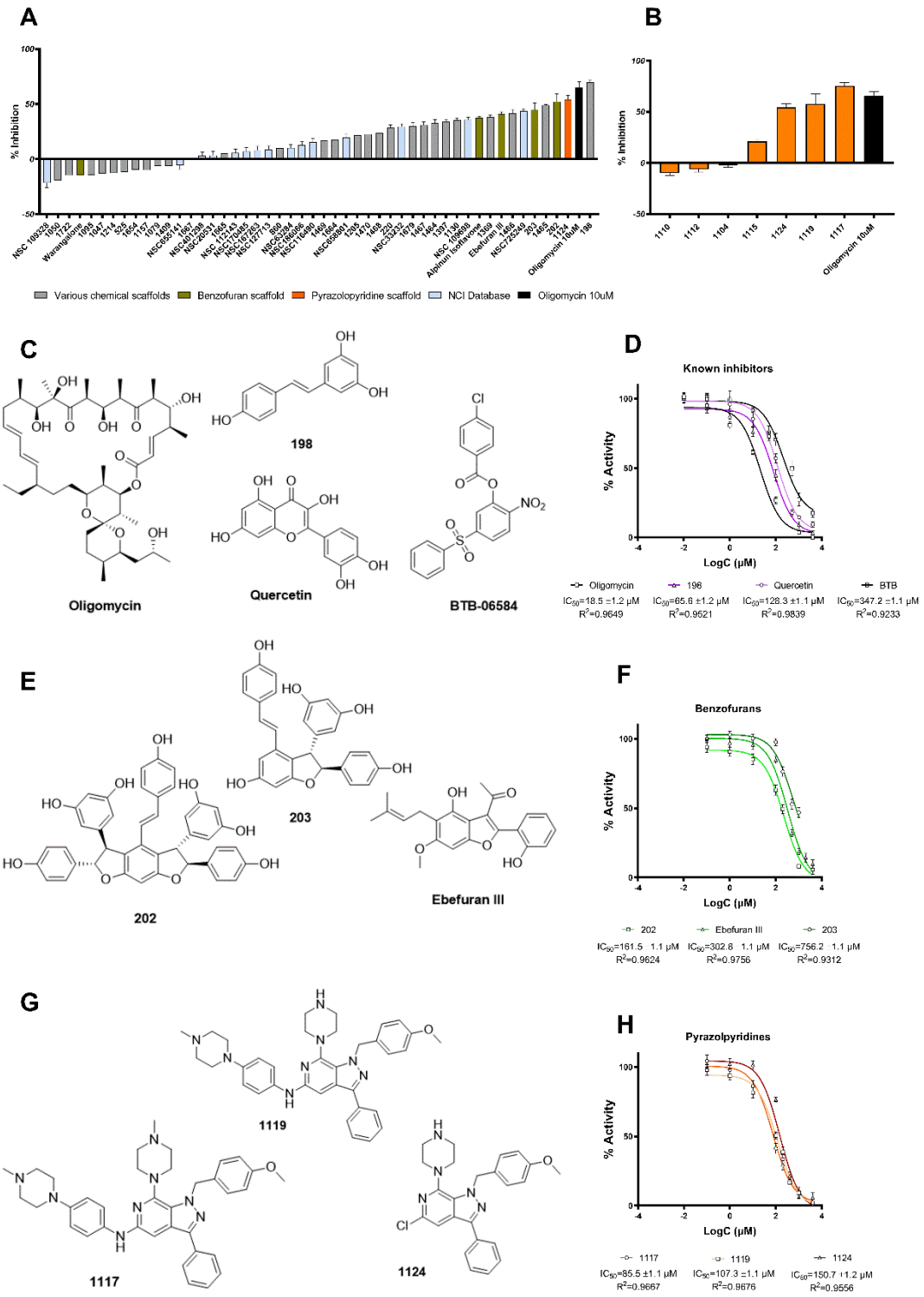

Figure 2: % Inhibition of the ATP hydrolase activity in isolated murine heart mitochondria. *In vitro screening evaluation of:* ***A)*** *the hits deriving from Pharmalab and the NCI library and* ***B)*** *the pyrazolopyridine-bearing compounds of Pharmalab at a concentration of 200μM. The orange and the green color denote the candidates with a pyrazolopyridine and benzofuran scaffold respectively while the NCI database molecules are denoted with light blue. Oligomycin was used as a positive control and tested at 10μM. The candidates with over 40% inhibition in the screening and the NCI molecules were evaluated using n=3 independent biological replicates.*

*Bar plots demonstrate mean± SD. Chemical structures of **C)** known non-selective inhibitors ATPase inhibitors,* **E)** *candidates with a benzofuran scaffold and **G)** candidates with a pyrazolpyridine scaffold. IC_{50} values against ATP hydrolysis in isolated murine heart mitochondria of **D) oligomycin,** compound **198, Quercetin** and **BTB.*** **F)** *compound **202**,**203** and **Ebefuran III**, **H)** compounds **1117**,**1119** and **1124**. Dot plots and error bars indicate mean and SD from n=3-5 biological replicates. The IC_{50} values were calculated based on the log(inhibitor) vs. normalized response least squares fit model of GraphPad Prism 8 software.*

b) Biological evaluation of the hit pyrazolopyridine compounds

To evaluate the effect of the inhibitors on ATP hydrolysis at a cellular level and to examine their selectivity for inhibiting hydrolysis over synthesis of ATP, we used a cellular assay in which H9c2 cells are first loaded with a dequenching concentration of tetramethylrhodamine (TMRM) then treated with rotenone. Rotenone inhibits complex I of the electron transport chain, leading to a reversal in the ATP synthase activity. The addition of an ATP hydrolase inhibitor in the presence rotenone leads to mitochondrial depolarization and release of the TMRM dye in the recording buffer, which is detected under these experimental conditions as an increase in the fluorescence (here reported as rate of fluorescence increase) (*Figure 3A*).[21] This increase is indicative of the inhibition of ATP hydrolysis by the F_1F_O-ATP synthase (*Figures 3B, 3C and 3D*). If a decrease in TMRM fluorescence is seen when a test compounded is added in the *absence* of rotenone, this depolarization must result from non-specific cellular or mitochondrial toxicity. As was expected, the control compound oligomycin, which is known to inhibit ATP synthesis, reduced fluorescence (***p<0.001 vs Dimethyl sulfoxide; DMSO, *Figure 3D, 3E and 3F*). The novel inhibitors were tested at 3 different concentrations: 100µM, 50µM and 10µM. Upon the addition of rotenone, we found that **1117**, **1119** and **1124** at 100 µM significantly increased mitochondrial depolarization (p<0.001, p<0.01 and p<0.001 respectively) at similar levels as oligomycin (p<0.001). We also confirmed the inhibition of ATP hydrolysis by BTB (100µM) as previously reported[21] (*Figure 3B*). Moreover, **1117**, **1119** and **1124** at 50 µM significantly increased mitochondrial depolarization while BTB is inactive in this concentration

(*Figure 3C*) and therefore was not tested at lower concentrations. None of the inhibitors were effective at 10μM in inhibiting either the hydrolysis or synthesis of ATP (*Figures 3D and 3E,* respectively). A separate TMRM assay was conducted in the absence of rotenone, in which case an increase in TMRM fluorescence following test drug administration is caused by non-specific cellular or mitochondrial toxicity. Addition of **1117**, **1119** and **1124** at 100 μM significantly increased fluorescence indicative of cellular toxicity while BTB at 100μM did not alter mitochondrial potential (*Figure 3E*). The fluorescence was monitored in living cells in a kinetic manner and the respective fluorescence tracing for each experimental condition is depicted in *Supporting Information, Figure S2.* FCCP was added in the end of TMRM fluorescence monitoring and verified that mitochondrial depolarization causes an increase in TMRM fluorescence.

In order to verify that the increase in fluorescence at a resting state, correlates to the toxicity of the compounds, we performed a cell viability assay. In brief, H9c2 cells where exposed to the compounds at 100μM, 50μM and 10μM for one hour and the 3-(4,5-dimethylthiazol-2-yl)-2,5-diphenyl-2H-tetrazolium bromide (MTT) reagent was applied to determine cell viability. The MTT assay is a colorimetric assay for assessing cell metabolic activity in which the NAD(P)H-dependent cellular oxidoreductase enzymes convert MTT to its insoluble formazan, which has a purple color. The intensity of the colorimetric measurement reflects the number of viable cells present in the well. Our results, demonstrate that **1117** and **1124** at 100 μM significantly decreased survival ($p<0.0001$). **1119** and BTB also reduced cell viability to a lesser extent ($p<0.05$) (*Figure 3H*). At 50μM and 10μM we observed that only **1124** lead to a significant reduction in cell survival ($p<0.001$ and $p<0.01$ respectively) (*Figures 3I and 3J*). An altered mitochondrial potential was not observed with 50μM **1117** or 50μM **1119**, and furthermore they did not alter cell viability determined via MTT assay (*Figure 3I*), which indicates that these two molecules are more effective than BTB, non-toxic

and selective at this concentration. In contrast, the toxicity of **1124** pertains at 50μM (*Figures 3F and 3I*). An increase in TMRM fluorescence in absence of rotenone was no observed by none of the compounds 10uM (*Figure 3G*).

We observed that the cellular toxicity is in accordance with the data of TMRM fluorescence increase with the exception of the BTB at 100μM and **1124** at 10μM in which the TMRM fluorescence was not significantly altered while the MTT assay demonstrates slight, but significant toxicity (*Figure 3H and 3J*). This discrepancy may be attributed to the sensitivity of the two methods or to parallel mechanisms that blunt mitochondrial metabolism without affecting deltapsim. Since, these molecules were not selected for optimization, we did not further investigate the mechanism of cell survival.

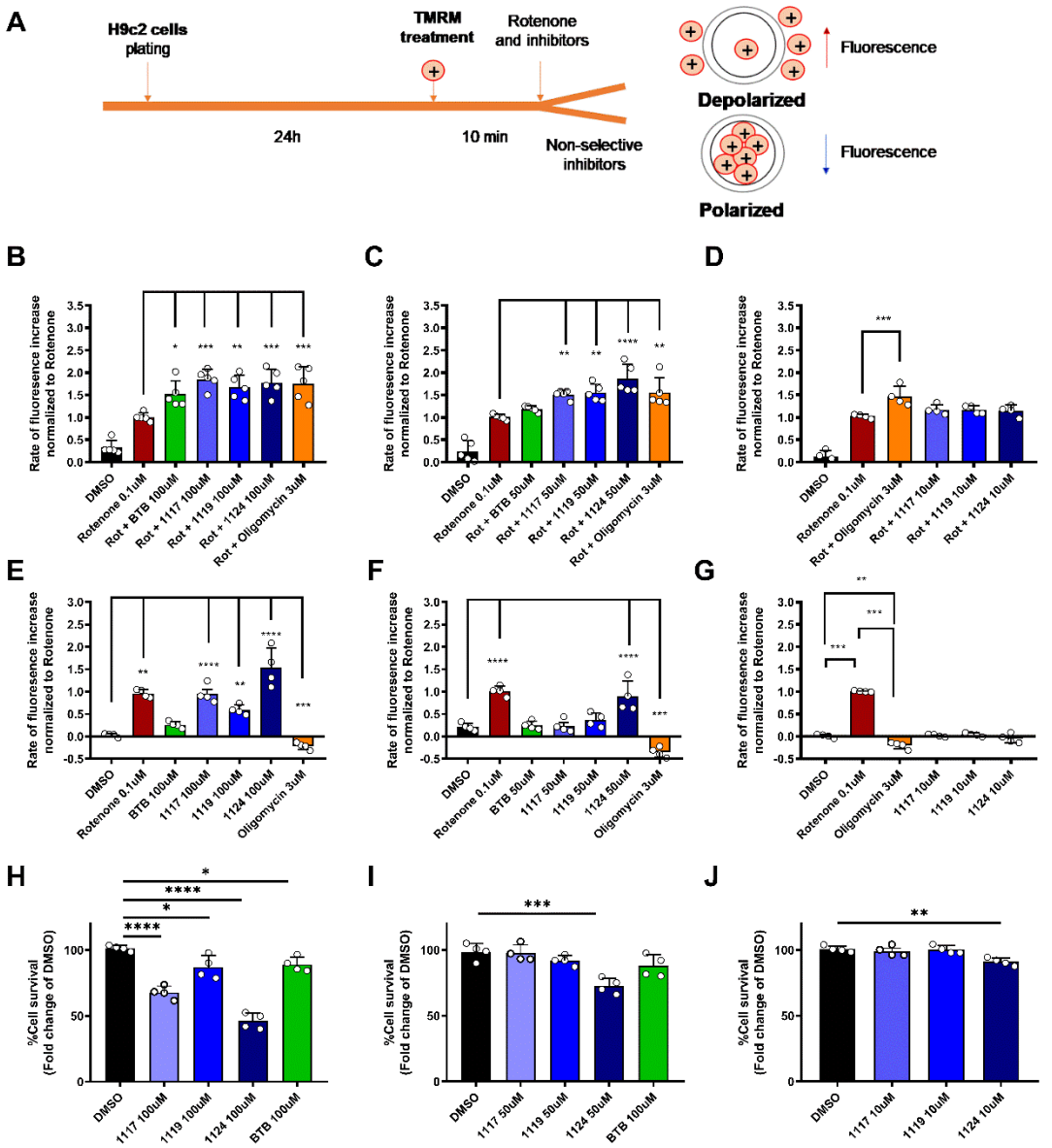

Figure 3: Evaluation of ATP hydrolysis and synthesis inhibition on H9C2 cells*. **A)**The experimental protocol in vitro indicating the localization of TMRM dye depending on the polarization of the cell upon the treatment with the inhibitors. On the left panel bar plots depict the rate of TMRM fluorescence increase upon treatment with BTB and pyrazolopyridine inhibitors (**1117**,**1119**,**1124**) normalized to rotenone at a concentration of **B)**100μM, **C)** 50μM and **D)**10μM. Rotenone (Rot) 0.1μM was added simultaneously with the inhibitors in order to induce the reverse activity of the ATP synthase. On the right panel bar plots depict rate of TMRM fluorescence increase when rotenone was not added to the experimental setting with the inhibitors and therefore the specificity or the toxicity of the compounds towards the hydrolase activity was examined. The graphs demonstrate the effect of treatment with BTB and pyrazolpyridine inhibitors (**1117**,**1119**,**1124**) at **E)**100μM, **F)** 50μM and **G)**10μM. % Cell survival of H9c2 cells upon exposure to the compounds for 1h at a concentration of **H)**100μM, **I)** 50μM and **J)**10μM determined via MTT assay(n=4 independent experiments). One way ANOVA, Tukey's test (*p<0.05, **p<0.01,***p<0.001 and ****P<0.0001). Bars present mean ±SD (n=4).*

For these reasons, we selected **1117** and **1119** as leads for the synthesis of new derivatives. Moreover, we considered them as candidates for *in vivo* studies while **1124** was excluded from further evaluation. In any case, **1124** is a 5-chlorosubstituted derivative and this feature substantially differentiates it from its other two counterparts, which both are substituted at 5-position of the pyrazolopyridine scaffold with a 4-(4-methylpiperazin-1-yl)aniline moiety.

In the context of cardioprotection, the F_1F_O-ATP synthase has been suggested to be one of the major components/modulators of the mitochondrial permeability transition pore (mPTP).[32,33] The mPTP is a high-conductance channel in the inner mitochondrial membrane which responds to increased Ca^{2+} concentration, whose opening during early reperfusion ultimately leads to programmed cell death.[10,34] The c subunit of F_1F_O-ATP synthase could form the mPTP[35,36] and mPTP modulators targeting the F_1F_O-ATP synthase are currently under investigation for therapeutic interventions.[37,38] Recently, triazaspiro[4.5]decane derivatives were identified as mPTP inhibitors, interacting with the c subunit of the ATPase and they exhibited cardioprotective effect in terms of alleviation of myocardial damage.[39]

Therefore, we evaluated whether the pyrazolpyridine scaffold and our lead compounds affect mPTP opening. The derivatives **1117**, **1119** and **1124** were investigated at concentrations from 10mM to 10 μM using the mitochondrial calcium retention (CRC) assay, in which isolated mitochondria are challenged with sequential addition of Ca^{2+} until the mPTP opens (*Figure 4A*). Cyclosporin A (CsA) (1μg/mL) was used as a positive control and significantly increased mitochondrial CRC. Our results showed that the ATP hydrolase inhibitors **1117**, **1119** and **1124** do not alter the number of calcium pulses needed for mPTP opening (*Figures 4B, 4D and 4F*) and did not affect the opening of the mPTP (p=ns, of all inhibitor concentrations vs the control group, *Figure 4C,4E and 4G*). Furthermore, they did not affect the ability of CsA to inhibit the

mPTP, implying that binding of CsA was unaffected (p=ns, of the inhibitor+CsA compared to CsA alone, *Figure 4C,4E and 4G*). These findings suggest that **1117**, **1119** and **1124** do not act as mPTP desensitizers. MPTP pore opening can be stimulated by mitochondrial matrix Ca^{2+} accumulation, adenine nucleotide depletion, increased phosphate concentration or oxidative stress.[40] Along this line, translocator protein (TSPO) in the outer mitochondrial membrane protein has been shown to function in the transport of cholesterol into mitochondria. TSPO has also been considered as a structural component of the mPTP and several inhibitors of mPTP or tracers have been developed targeting TSPO[41,42]. A limitation in our study is that we did not examine the interaction of the pyrazolopyridine inhibitors with other inhibitors of mPTP besides CsA. However, since in our results the pyrazolopyridine inhibitors do not alter the opening of mPTP opening alone and our results are negative, the addition of other known inhibitors was not performed.

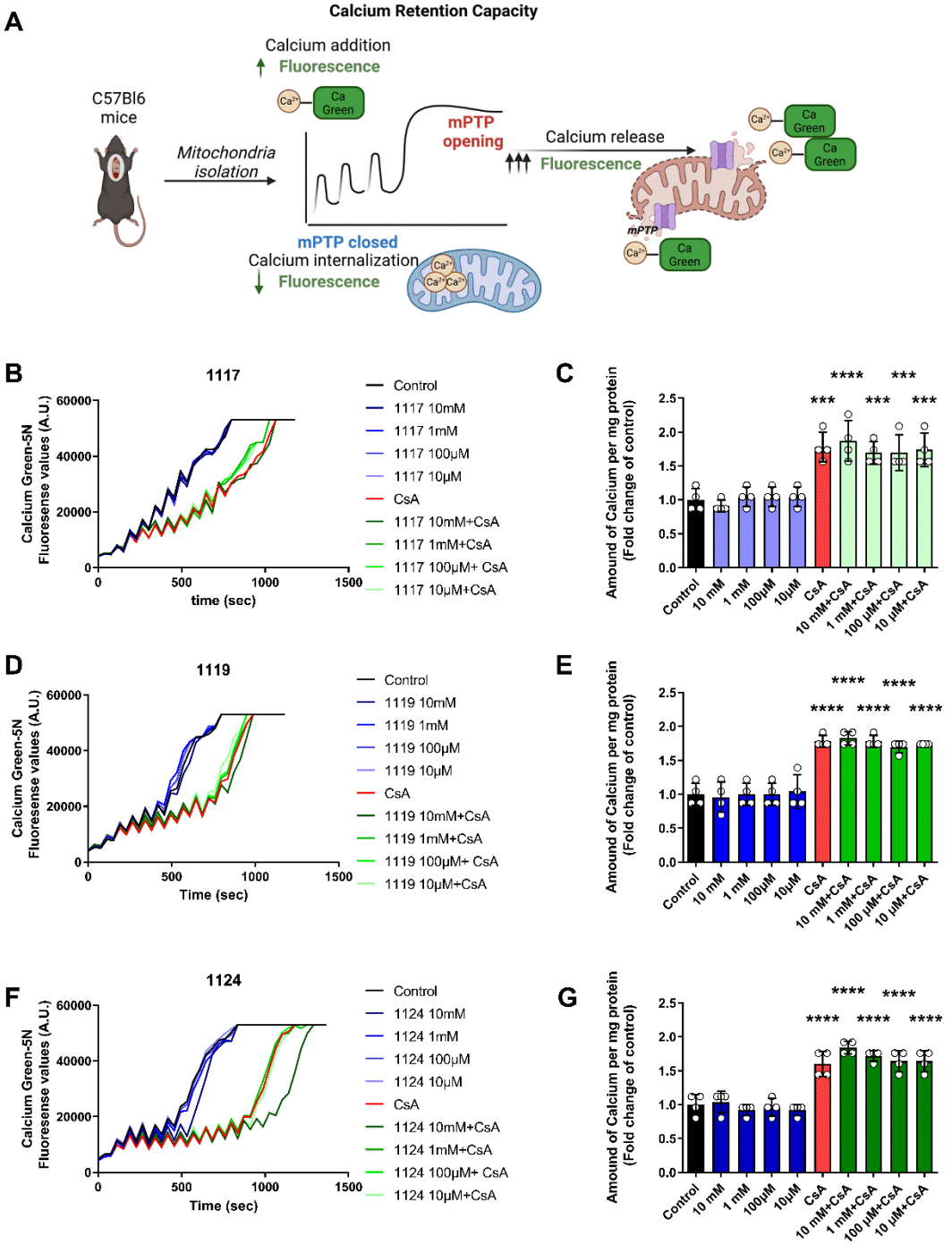

Figure 4: 1117, 1119 and 1124 do not suppress mPTP opening on murine heart mitochondria. A) *CRC was determined on isolated murine heart mitochondria treated with inhibitors and compared to those treated with vehicle (DMSO) based on the number of calcium pulses needed for mPTP opening.* ***B, D, F)****: The graphs represent the fluorescence tracing of the extramitochondrial calcium.* ***C, E, G)****: None of the ATP hydrolysis inhibitors increases mitochondrial calcium uptake. One way ANOVA, Tukey's test (***p<0.001 and ****p<0.0001, of CsA treated groups compared to respective concentration of the inhibitor without CsA). Bars present mean ±SD (n=4 biological replicates).*

c) Hit optimization and in vitro evaluation.

Based on the structure of **1117** and **1119** and considering the afore mentioned biological results, we decided to further study this scaffold, thus we designed a number of new modified derivatives. We estimated that the 4-(4-methylpiperazin-1-yl)phenylamino substituent, present at position 5- of both **1117** and **1119** plays an important role to the interaction with the enzyme, consequently we preserved this substituent in all new synthesized compounds and we inserted modifications with various electronic and/or steric properties at positions 1, 3 and 7 of the central scaffold. More precisely, we introduced a methyl or a 4-methoxybenzyl group at position 1, a phenyl or a 3-fluorophenyl group at position 3 and an arylether or an alicyclic amine at position 7 (*Figure 5*).

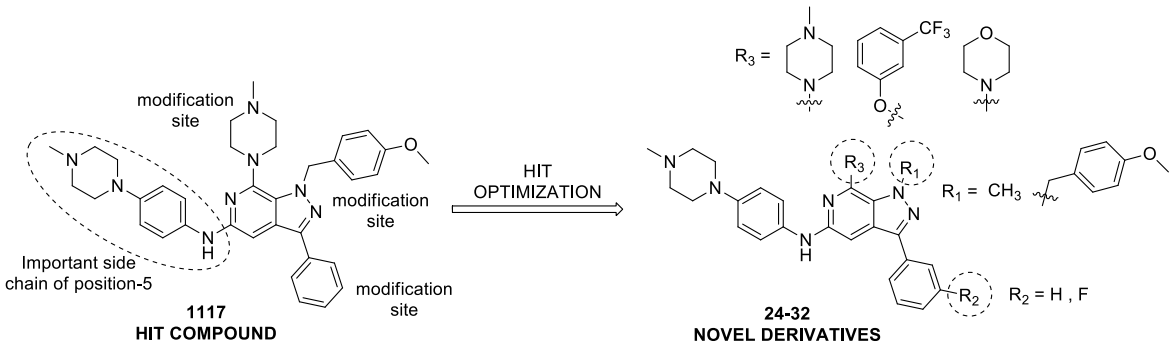

Figure 5: Rationale for hit optimization. *Structural modifications on the hit compound **1117** were performed by altering the substituents on positions 1, 3 and 7 of the pyrazolopyridine scaffold, resulting in the nine novel derivatives **24-32**.*

Nine new pyrazolo[3,4-c]pyridine derivatives, compounds **24**-**32**, were synthesized by following a synthetic procedure previously developed by our group[43,44] and depicted in *Scheme 1.*The synthesis of the new compounds was performed using as starting materials the substituted pyrazolopyridines **1** and **2**, which we have previously reported.[43,44] Each compound underwent a Suzuki type coupling using two boronates and provided the 3-phenylsubstituted derivatives **3** and **4,**[43,44] as well as the new fluorosubstituted analogues **5** and **6**. These derivatives were first converted to the

corresponding *N*-oxides **7**-**10** and then, following a rearrangement, to the 5,7-dichlorides **11**-**14** *(Scheme 1).* Among them, compounds **8** and **12** are previously reported derivatives .[43]

The 1-methyl substituted derivatives **11** and **13** were treated with *N*-methylpiperazine or 3-trifluoromethylphenol to give the 7-substituted analogues **15**-**18** (*Figure 5B of the manuscript*). In the case of the 1-(4-methoxybenzyl)-substituted derivatives **12** and **14** we have additionally used morpholine and prepared the corresponding derivatives **19**-**23**. Each of the above mentioned chlorides reacted with 4-(4-methylpiperazin-1-yl)aniline[73] in the presence of $CsCO_3$, X-Phos and $Pd(dba)_2$ to result in the target compounds **24**-**32** (*Scheme 1*). A detailed description of the synthesis and characterization of the novel compounds is provided in the Experimental Section and the copies of their ^{1}H- and ^{13}C-NMR spectra are presented in the Supporting Information file. Prior to *in vitro* evaluation, all newly synthesized compounds were filtered for Pan Assay Interference through web server PAINS-Remover (https://www.cbligand.org/PAINS/)[46] showing no possible PAINS activity.

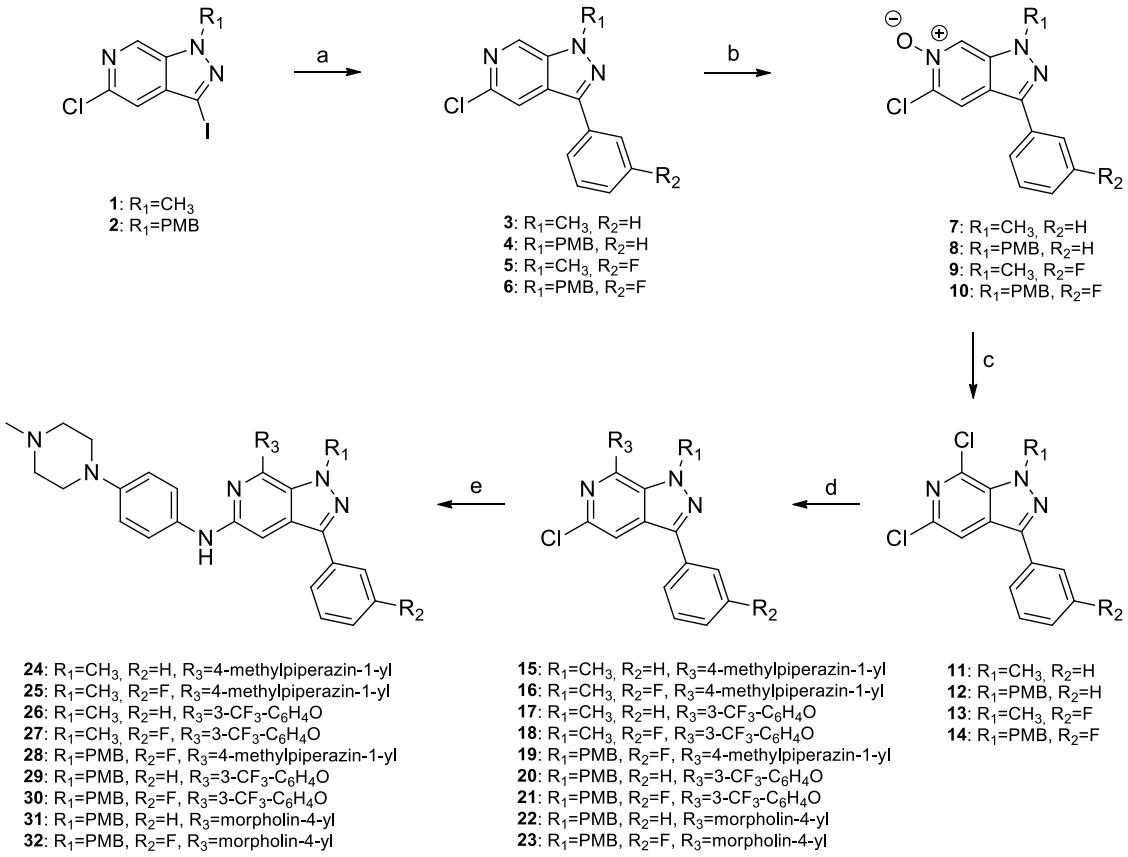

Scheme 1: Reagents and conditions for the synthesis of the novel compounds 24-32*. Reagents and conditions. a: phenylboronic acid or 3-fluorophenylboronic acid, $Pd(PPh_3)_4$, $NaHCO_3$, toluene/EtOH/H_2O, 100 ^oC, Ar, 20-30 h, 87-100%; b: 3-chloroperbenzoic acid, CH_2Cl_2, 48 h, 48-65%; c: $POCl_3$, THF dry, 12 h, 84-95%; d: 4-methylpiperazine, or morpholine, or 3-trifluoromethylphenol/K_2CO_3, DMSO, Ar, 130-160 ^oC, 20-150 min, 50-95%; e: 4-(4-methylpiperazin-1-yl)aniline, $CsCO_3$, X-Phos, $Pd(dba)_2$, toluene dry, reflux, 18-20 h, 20-75%*

The new compounds **24**-**32** were evaluated for their inhibitory effect on F_1F_O-ATP synthase hydrolytic activity. For comparison reasons, the 5-chlorosubstituted intermediate **22** (*Scheme 1*) was also included in the initial evaluation. Compounds **28**, **31** and **32** inhibited the ATP hydrolysis at 200μM (*Figure 6A and Supporting Information, Table S4*). The results of the initial screening indicated that replacement of the 4-methoxybenzyl group at position -1 of the pyrazolopyridine scaffold with a methyl group resulted in the loss of the inhibitory activity (compounds **24** and **25** vs 1117).

Nevertheless, when an aromatic substituent was incorporated at position -7 instead of the 4-methylpiperazine moiety, the corresponding N1-methylated analogues **26** and **27** proved to partially regain the inhibitory activity. On the contrary, the presence of a morpholine group at position -7 or the 3-fluorophenyl substituent is well tolerated (compounds **31**, **32** and **28**, respectively), leading to the most active derivatives among the newly synthesized compounds.

The IC_{50} values of the most promising new compounds were determined. Compound **31** exhibited similarly low IC_{50} as compounds **1117** and **1119** (98.5±1.1μM) (*Figure 6B*). The other two candidate inhibitors, **28** and **32** exhibited higher IC_{50} values. Among these two compounds, **28** exhibited comparable inhibition with **1124** (IC_{50} =163.7 ± 1.1) whereas compound **32** was excluded from further analysis due to the much higher IC_{50} value (1977 ± 1.2) (*Figure 6B*). Compound **28** did not exhibit considerable inhibition since even in the highest concentration did not result in over 50% inhibition. Since the IC_{50} Curve does not reach the plateau, the IC_{50} calculation of **28** is questionable.

The selected derivatives **31** and **28** (*Figure 6C*) were further evaluated *in vitro* on the H9c2 cells and the membrane potential was monitored in the presence and in the absence of rotenone. Upon rotenone treatment, compound **31** at 100μM and 50μM resulted in a significant increase in mean fluorescence, indicating the inhibition of the ATP hydrolysis (*Figure 6D*). This compound proved to be also not toxic in none of the tested concentrations and did not inhibit the synthesis of ATP as indicated by the membrane potential in the absence of rotenone (*Figure 6E*). In fact, compound **31** exhibited similar inhibition on ATP hydrolysis as **1117** and **1119** and an improved profile in terms of cellular toxicity. When ATP hydrolysis was reversed by rotenone, compound **28** significantly amplified the rate of increase of fluorescence at 100μM, 50μM and 10μM (*Figure 6C*). However, this compound also increased fluorescence at a resting state at 100μM and 50μM indicating cellular toxicity (*Figure 6E*) and thus it was excluded from further evaluation. The fluorescence was monitored in living cells

in a kinetic manner and the respective fluorescence tracing for each experimental condition is depicted in *Supporting Information, Figure S3.* FCCP was added in the end of TMRM fluorescence monitoring and the depolarization of cells was evident by the TMRM fluorescence increase.

Moreover, we conducted a cell viability test via MTT assay and we found that compound **28** decreased cell viability in all the tested concentrations ($p<0.001$) while compound **31** did not result in alterations of cell survival (*Figure 6F*). This finding is concomitant with TMRM increase in the absence of rotenone and confirms the cellular toxicity of compound **28**.

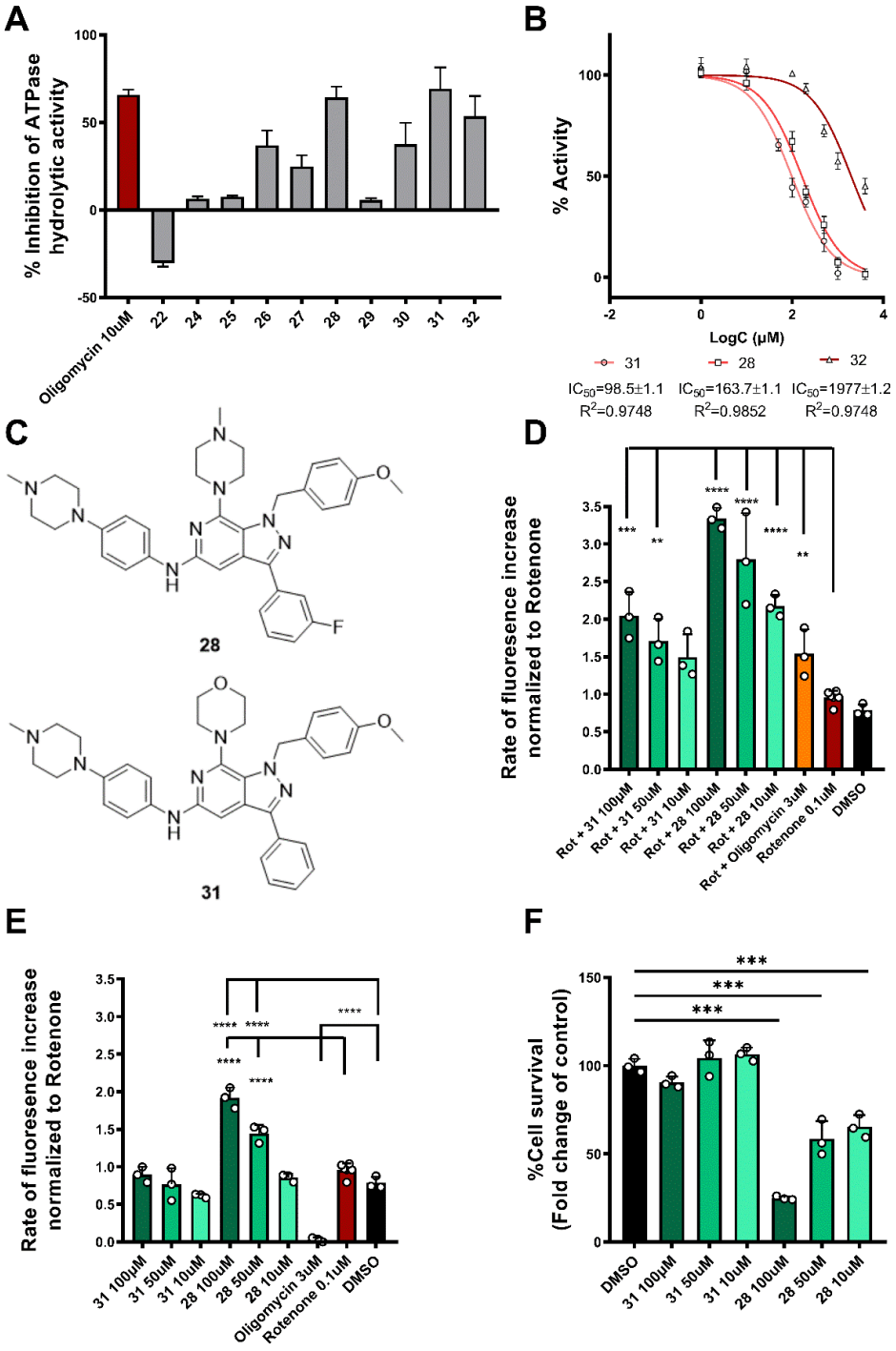

***Figure 6: In vitro evaluation of the new pyrazolpyridine derivatives**. **A)** % Inhibition of the ATP hydrolase activity in isolated murine heart mitochondria by the newly synthesized compounds at 200µM. **B)** IC_{50} values of the new compounds **31**, **28** and **32** against ATP hydrolysis. The IC_{50} values were calculated based on the log(inhibitor) vs. normalized response least squares fit model of GraphPad Prism 8 software. **C)** Chemical structures of the new compounds **31** and **28**. **D)** Rate of TMRM fluorescence increase upon treatment with **31** and **28** normalized to rotenone.*

Rotenone (Rot) 0.1μM was added simultaneously with the inhibitors in order to induce the reverse activity of the ATP synthase. ***E)*** *Rotenone was not added to the experimental setting with the inhibitors and therefore the specificity or the toxicity of the compounds towards the hydrolase activity was examined.* ***F)*** *% Cell survival of $H9C_2$ cells upon exposure to the compounds for 1h determined via MTT assay. One way ANOVA, Tukey's test (**p<0.01,***p<0.001 and ****P<0.0001). Bars present mean ±SD (n=4 biological replicates).*

The design, synthesis and biological evaluation of nine novel pyrazolopyridine derivatives revealed the optimal features in the chemical structures that are related to the inhibition of the reverse activity of F_1F_O ATP synthase, contributing to structural activity relationships. Based on our results, we deduce that the 4-methoxybenzyl group at position 1 of the pyrazolopyridine scaffold is important for the inhibition of the reverse activity of F_1F_O ATP synthase since its replacement with a methyl group resulted in the loss of the inhibitory activity. Moreover, the presence of a morpholine group at position 7 led to the most active derivative among the newly synthesized compounds.

Creation of a holistic structure model of the *Mus musculus* F_1F_O ATP synthase and pyrazolopyridine compound 31 binding mode

In order to investigate the binding mode for our new synthesized compounds we constructed a holistic model of ATP synthase of *Mus musculus* containing all different subunits, based on homology modeling (*Figure 1B and Figure 7A)*, utilizing all known structural data from Protein Data Bank (PDB) (see experimental section). The finally tested (*Figure 6A*) 10 synthesized compounds were *in silico* examined against resveratrol/quercetin and aurovertin B binding pockets. Induced-Fit Docking (IFD) simulations were carried out to reveal possible mode of binding in both binding sites. On global minimum structure for each complex, theoretical MM-GBSA binding energy was calculated, as implemented on Schrodinger Suite 2022. The binding energy was correlated with the % inhibition of the ATP hydrolase activity in isolated murine heart mitochondria. For resveratrol/quercetin binding pocket the correlation

Pearson *r* was calculated -0,7529, while for aurovertin B pocket the correlation was calculated -0,7079 (*Supporting Information, Table S5 and Figure S4*).

To validate our theoretical docking models, quercetin was submitted to IFD calculations, and the resulted structure is in very good agreement with the crystallographic one on F_1F_O-ATP synthase from bovine heart mitochondria (PDBid: 2jj2, *Supporting Information, Figure S5*) confirming our approach.

The very good agreement between theoretical and experimental activity prompt us to hypothesize that the newly synthesized pyrazolopyridines inhibit F_1F_O-ATP synthase by binding to the resveratrol/quercetin cavity. Thus, focusing on compound **31** which exhibited the most favorable pharmacological profile *in vitro*, IFD calculations showed that its binding mode is similar to quercetin and resveratrol (*Figure 7 and Supporting Information, Figure S5*), yet several interactions can explain the observed experimental difference in activity. Compound **31** is extended in the binding cavity forming from one side a salt bridge between 4-methylpiperazin fragment with E289 and on the other side a hydrogen bond formed between the O-Me group with the side chain of T278, while the morpholine group is accommodated in a hydrophylic cavity surrounded by R277, D366, E355 and R334 (*Figure 7C and E and Supporting Information, Figure S5A*). Interestingly, the major difference between resveratrol/quercetin and compound **31** are the strong interactions formed by the latter with E289 and T278, both residues belonging in the C-terminal part of *γ*-subunit. Compared to quercetin crystal structure (*Figure 7B and 7D)* with bovine F_1F_O ATP synthase (PDBid: 2jj2[18]) both molecules lay in the same orientation in the cavity with the core aromatic rings surrounded by the hydrophobic residues A278, V279, I263, A256 (*Supporting Information, Figure 5B*), and the same holds for resveratrol (pdb 2jiz *not shown*). The exact rotary mechanism for ATP hydrolysis and synthesis in the F_1F_O-ATP synthase as well as the endogenous modulators of the processes are not fully understood. Very recently, the possible molecular mechanism for the IF_1 inhibition of ATP hydrolysis was identified, were the interaction with the *γ*-subunit of the F_1F_O-ATP

synthase with the N-terminal regions of IF_1 was found important for the rotational-direction-dependent function of the enzyme.[47] It is also known that the orientation of *γ*-subunit is important for ATP binding on the catalytic site of *β* subunit[48] since rotation of *γ*-subunit by 200 degrees results in the hydrolysis of ATP to ADP and *Pi*. Via our IFD simulations, we concluded that the pyrazolopyridine ATP hydrolysis inhibitors interact with the resveratrol/quercetin cavity. We assume that the specific interactions of compound **31** take place in this cavity of the *γ*-subunit, prevent counterclockwise rotation and explain **31**'s selectivity on ATP hydrolysis inhibition.

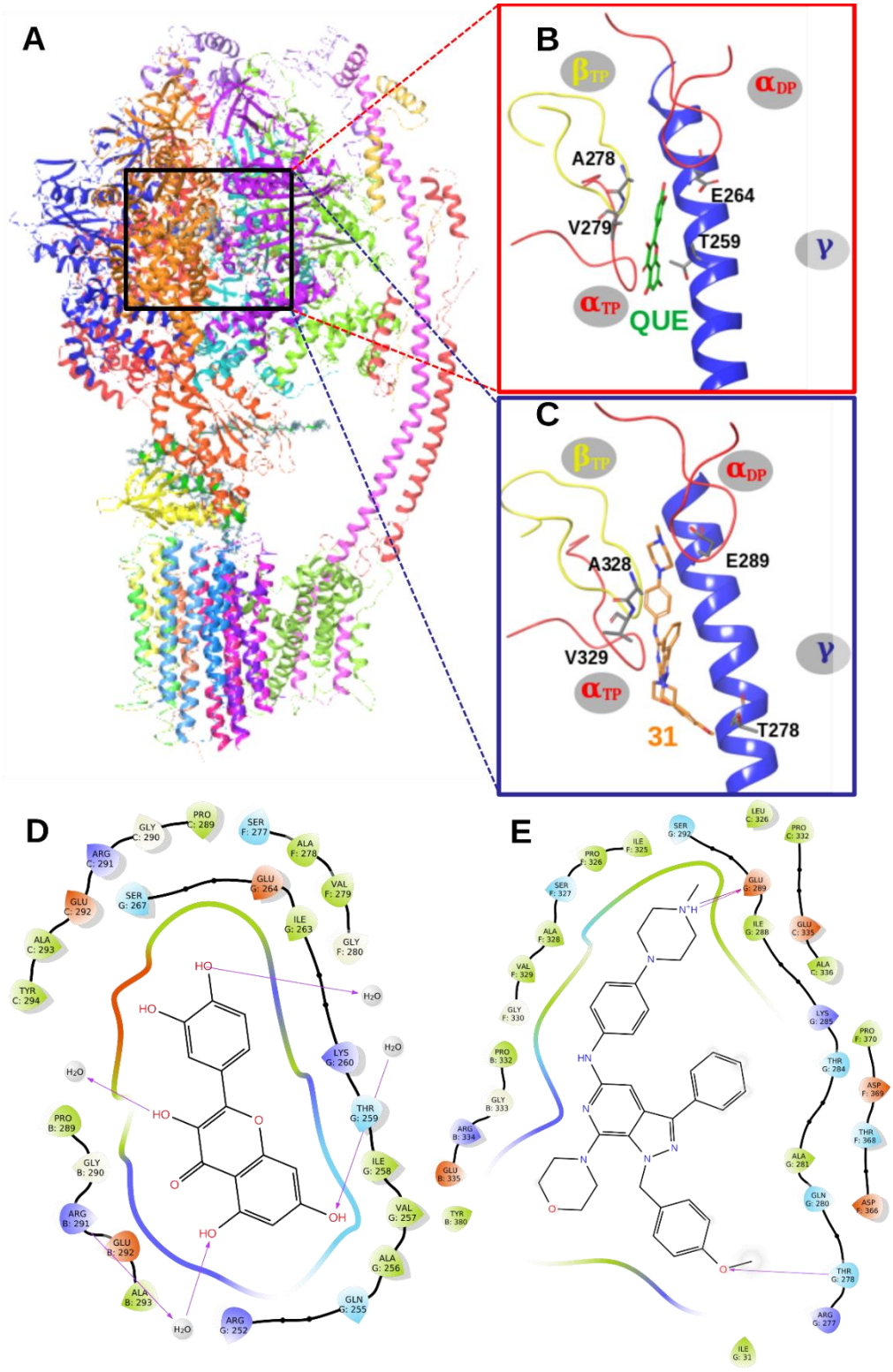

Figure 7: F_1F_O -ATP synthase model and interactions of compound 31 with γ subunit. A) *Homology model of Mus musculus F_1F_O ATP synthase.* ***B)*** *Crystal structure of quercetin bound to bovine ATP synthase among α-. β- and γ- subunits (PDBid: 2jj2).* ***C)*** *Theoretical binding mode of compound* ***31,*** *among, α-, β- and γ-subunits. The α-, β- and γ-subunits are red, yellow, and blue, respectively, and ligand is green.* ***D, E)*** *2D interaction diagrams of* ***B*** *and* ***C*** *respectively. Quercetin interacts with γ-subunit through hydrophobic contacts with the helix and through water bridges. Compound* ***31*** *embraces extensively γ-subunit forming hydrophobic interactions and*

more importantly a salt bridge between piperazine moiety and E289 and a hydrogen bond between p-ethoxybenzyl moiety and T278.

Inhibition of ATP hydrolysis as a target for cardioprotection *in vivo*

The promising biological activity of the pyrazolopyridine compounds prompt us to further evaluate *in vivo* compounds **1117**, **1119** and the novel compound **31** which were more effective than BTB in inhibiting ATP hydrolysis. We implemented an *in vivo* murine model of 30 minutes of ischemia and 2 hours of reperfusion in order to examine the cardioprotective effect of ATP hydrolase inhibitors[25] and we compared their IS limiting effects with those of BTB. In brief, twenty-five adult healthy C57Bl/6 mice 3 months old were randomized to receive intravenously the inhibitors **1117**, **1119**, BTB and **31** or the vehicle solution 5 minutes prior to the induction of ischemia (*Figure 8A*). The rationale for the administration of the inhibitors prior to ischemia was based on fact that ATP synthase reverses its activity when the oxygen supply is compromised[49]. The administration prior to ischemia allows the compounds to reach the ischemic region of the heart and exert their possible protective effects during the period of ischemia.[50] The dose of **1117**, **1119** and **31** was determined based on the effective concentration of 50 μM *in vitro* while for BTB the dose was higher since 100μM were needed at a cellular level to inhibit the ATP hydrolysis**.** Our results demonstrated that the administration of the hydrolase inhibitors **1117**, **1119** and **31** significantly reduced myocardial IS (%I/R 34.8 ± 1.5, 33.4 ± 2.1 and 25.6 ± 2.2 respectively *vs* 45.4 ±1.8 for the control group) (*Figure 8B*) when they administered prior to ischemia. BTB did not significantly reduce IS (%I/R 39.6 ± 1.8, p=ns *vs* the control group). All groups had similar risk/all myocardium areas (p=ns) (*Figure 8C*). Therefore, the inhibitors that derived from our screening and the newly synthesized inhibitor **31** exhibited enhanced *in vivo* efficacy compared to the previously described small molecule hydrolysis inhibitor BTB. We must underline herein that to the best of our knowledge BTB has not been previously tested in an *in vivo* setting. The explanation for the lack of efficacy of

BTB *in vivo* may rely on the fact its mode of action is via the IF_1 protein.[21] A recent study has shown that IF_1 is downregulated in the ischemic heart[51] and probably the mode of binding does not allow BTB to exert cardioprotective properties. Alternatively, it may be related to differing pharmacokinetics or pharmacodynamics.

Compound **31** exhibited the higher cardioprotective effect and therefore this new compound was chosen for further studies and was administered 5 minutes and 25 minutes after the induction of ischemia in the murine model of IRI (*Figure 8D)*. Treatments that are applied after the onset of ischemia, may reach the border zone of infarction and to a lesser extend the ischemic region via the collateral circulation since the heart is already ischemic.[50] The interventions performed after the onset of ischemia may exert their cardioprotective mechanism both at the ischemia and reperfusion phase. The rationale for the design of these experimental protocols lies on the fact that the administration at the 5th min of ischemia would allow compound **31** to exerts its protective effects during the ischemic period while the administration at the 25th min of ischemia would provide insights on whether its cardioprotective effects also occurs during the first minutes of reflow.[25,50] Additionally, these two experimental protocols mimic the clinical praxis since the administration early at ischemia or prior to reperfusion could be performed prior or during the percutaneous coronary intervention in patients undergoing AMI.[8,25]

The administration of compound **31** significantly reduced IS when was administered at the 5th min after the induction of ischemia (%I/R 23.1 ± 3.7 *vs* 45.0 ± 2.2 for the control group, ***p=0.0009) (*Figure 8E*). Both groups had similar risk/all myocardium areas (p=ns) (*Figure 8F*). On the contrary, when compound **31** was administered late at the 25th minute of ischemia, just before the onset of reperfusion, its important cardioprotective effect is lost since we observed only a trend in the reduction of IS (%I/R 40.4 ± 3.2 *vs* 47.8 ± 3.4 for the control group, p=0.1486) (*Figure 8E*).

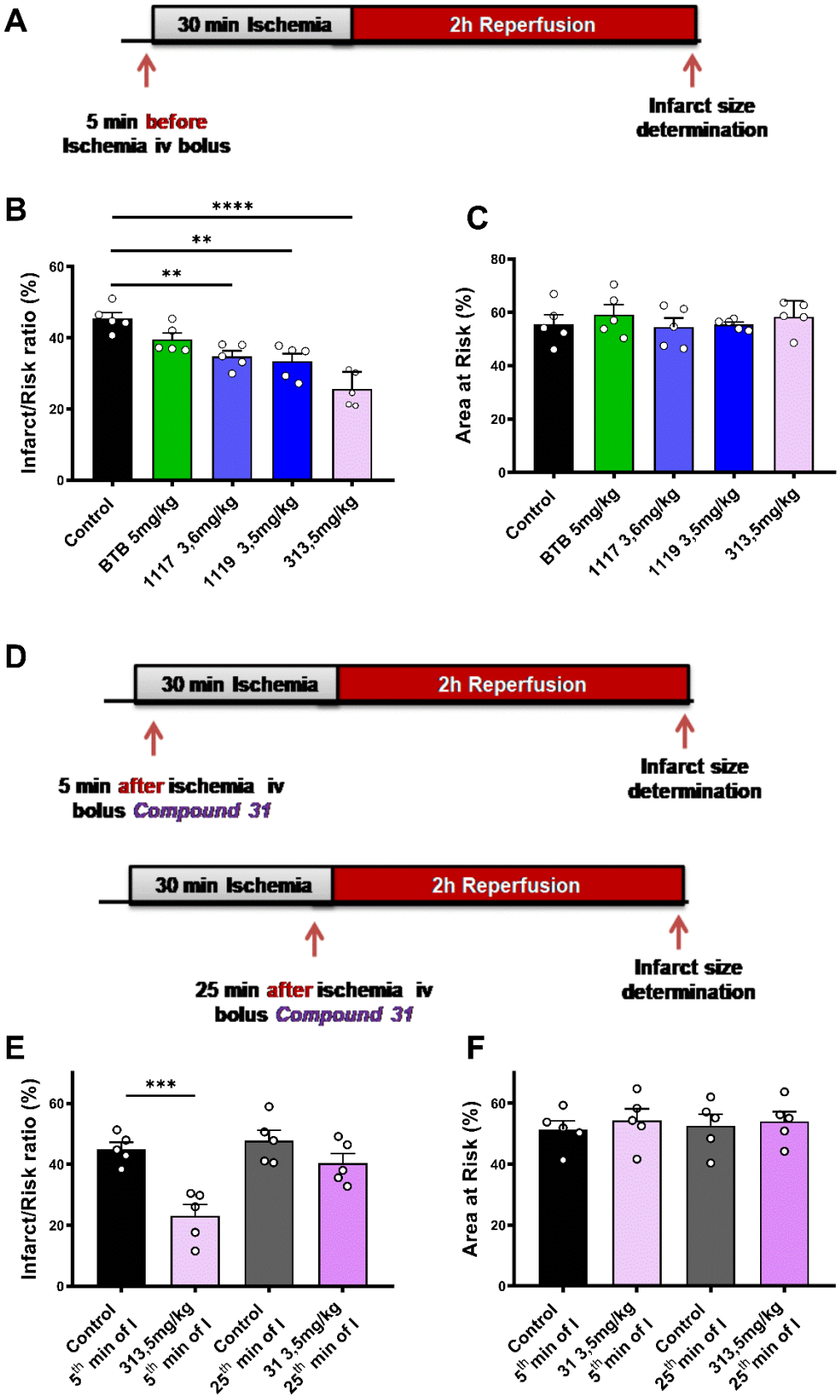

***Figure 8**: **The ATP hydrolase inhibitors are cardioprotective when given before or early during ischemia. A)** In vivo experimental protocol: The inhibitors are given 5 minutes (min) prior to ischemia in order to compare the cardioprotective effect*

of ATP hydrolysis inhibitors in terms of infarct size reduction. ***B)*** *Bar plot with the IS as determined by the % infarct to risk ratio and* ***C)*** *Bar plot of the % Area at risk after 30 minutes I and 2 hours of R. One way ANOVA, Tukey's test (**p<0.01and ****p<0.0001). Bars present mean ±SEM (n=5 animals per group).* ***D)*** *In vivo experimental protocol where Compound 31 and the vehicle control are administered 5 minutes and 25 minutes after the induction of ischemia* ***E****) Bar plot with the % infarct to risk ratio and* ***F)*** *% Area at risk of the compound* ***31*** *vs the control when the administration is performed (Unpaired t-test was performed for each timepoint, ***p<0.01). Bars present mean ±SEM (n=5 animals per group).*

Cardioprotective mechanism of the best ATP hydrolase inhibitor

Since compound **31** was most potent at reducing myocardial IS when it is administered prior to ischemia and reduced IS when it was administered at the 5th min of ischemia, we aimed to explore the underlying molecular cascades of cardioprotection *in vivo*. The experimental protocol was repeated with the administration of compound **31** at the 5th minute of ischemia, and the ischemic left ventricle was collected at the 10th minute of R (*Figure 9A*) as at this timepoint we have previously demonstrated the activation of cardioprotective pathways.[10,52] We first evaluated the ATP content of the tissue in order to examine whether at this timepoint of reperfusion ATP content is compromised by ischemia and if the administration of compound **31** leads to ATP content alterations. ATP preservation has been associated with cardiac protection from the ischemic injury both in *in vitro* and *ex vivo* models[53,54]. We measured the ATP content both in the ischemic and non-ischemic myocardium. Our results suggest the ATP concentration is reduced in the ischemic myocardium of the control group in comparison to the respective non-ischemic part indicating that ATP content has not been restored at early reperfusion ($p<0.01$) (*Figure 9B*). Moreover, we found that compound **31** leads to a significant increased ATP concentration in the ischemic tissue compared to the ischemic tissue of the control group ($p<0.05$) and the ATP levels were similar to the non-ischemic tissue of the control and compound **31** group ($p<0.05$) (*Figure 9B*).

ATP abundance leads to the activation of the P2Y receptors which are G-protein coupled receptors and are responsible for the activation of intracellular second

messenger systems to modulate Ca^{2+} mobilization from intracellular stores[55] or activate adenylate cyclase.[56] Therefore, at first we examined whether the inhibition of ATP hydrolysis may activate the signaling of the purinergic P2Y receptors in cardiomyocytes.[57] We evaluated the downstream activation of the cAMP-dependent protein kinase A (PKA) which is an ubiquitous enzyme that phosphorylates several soluble and membrane-bound substrates to confer cardioprotection.[58] Compound **31** increased the T173 phosphorylation and activation of PKA. PKA targets phospholamban (PLN), a membrane protein that inhibits the sarcoplasmic reticulum $Ca(^{2+})$-ATPase (SERCA).[59] In the unphosphorylated state, PLN binds to SERCA, reducing the calcium uptake and generating muscle contraction.

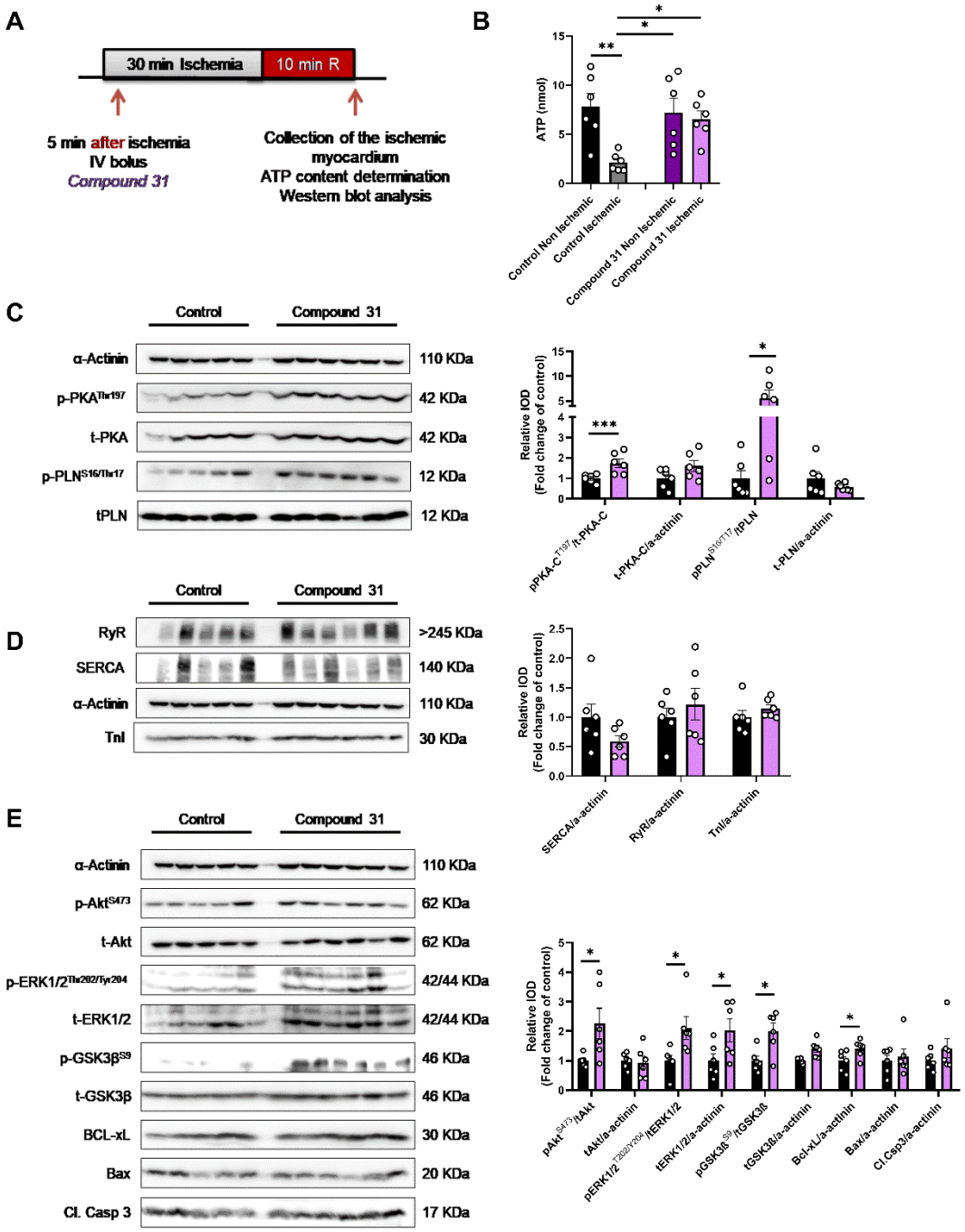

Figure 9: Cardioprotective mechanism of the ATP hydrolase inhibitor 31.A) *Experimental protocol for the elucidation of the cardioprotective mechanism of the ATP hydrolase inhibitor* ***31****.* ***B)*** *ATP content of the ischemic and non-ischemic myocardium. Relative densitometric graphs at the 10th min of reperfusion after normalization to total protein and representative Western Blots of* ***D****) phospho-(T197)-PKA/PKA, PKA/ α-actinin, phospho-(Ser16/Thr17) PLN/PLN and PLN/ actinin,* ***C****) SERCA/α-actinin, RYR/α-actinin and TnI/α-actinin and* ***E****) phospho-(S473)Akt/Akt, Akt/α-actinin, phospho-(T202/Y204) ERK1/2/ERK1/2, ERK1/2/ α-actinin, phospho-(S9) GSK3-β/GSK3-β, GSK3-b/ α-actinin, Bcl-XL/α-actinin, BAX/α-actinin and cl. Casp*

*3/α-actinin. Unpaired t-test (n=5-6 per group, *p<0.05 and ***p.0.001 vs the control group).*

Activation of PKA leads to the downstream phosphorylation S16/T17 of PLN at S16 in the cytoplasmic helix, relieving SERCA inhibition and initiating muscle relaxation. PLN once phosphorylated, it dissociates from SERCA and reduces intracellular Ca^{2+} levels by allowing it to pump Ca^{2+} back into the sarcoplasmic reticulum. In this way, the damage from Ca^{2+} overload is alleviated.[7,60] It has been proposed that PLN directly interacts with mitochondria and the endo/sarcoplasmic reticulum via the HS-1 associated protein X-1 (HAX1) regulating apoptosis.[61] We found that compound **31** led to the increased S16/T17 phosphorylation of PLN (*Figure 9C*), indicating that may reduce Ca^{2+} overload and inhibit apoptosis.[62] Compound **31** did not alter the expression of PKA, PLN, SERCA and ryanodine receptor (RYR) *(Figure 9C and 9D*) which means that the PKA and PLN pathway are transiently activated via phosphorylation when ATP hydrolysis is inhibited but are not upregulated via alterations in proteinosythesis.[63] Moreover, the protein levels of troponin I (TnI), which is the subunit of myocardial troponin responsible for the inhibition of actomyosin interaction were not different between the groups (*Figure 9D*) indicating that compound **31** did not affect the excitation-contraction coupling of the contractile mechanism of the cardiac muscle.[64]

Several pathways have been proposed to exert cardioprotective effects and the Reperfusion Injury Salvage Kinase (RISK) pathway emerged as a concept including certain pro-survival anti-apoptotic protein kinases, the original members of which were Akt and ERK1/2, which when specifically activated early at the time of myocardial reperfusion conferred powerful cardioprotection.[65–67] In parallel, several reports demonstrate the cross-talk between PKA and Akt activation[68–70] and for these reasons, in our next steps we evaluated the effect of compound **31** on the RISK pathway. The administration of compound **31** led to the significant increase in the phosphorylation and activation of Akt and ERK1/2 kinases in the ischemic myocardium at the 10th min

of reperfusion, compared to the Control group (*Figure 9E*). Moreover, to confirm the activation of RISK, we evaluated the downstream of Akt kinase, belonging to the RISK pathway, the Glycogen synthase kinase-3 beta (GSK3beta).[65] Our results showed that the activation of the RISK pathway by the administration of compound **31** is confirmed by the increased phosphorylation of GSK3beta at its inhibitory site S9 *(Figure 9E*). The protein expression levels of Akt, ERK1/2 and GSK3β were not altered (*Figure 9E*). It is well established that the short term activation of the pro-survival kinases belonging to the RISK pathway alleviates apoptosis and ultimately leads to the reduction in IS.[65]

The cell damage induced by IRI may lead to apoptosis, autophagy and necrosis, with the apoptotic cell death being the major determinant of lethal cardiomyocyte injury.[71] Our results so far demonstrated that the administration of compound **31** led to the increased phosphorylation of PLN and the activation of RISK pathway. These two pathways share a common feature: their activation converge on a decrease in apoptosis in the myocardium[62,65,72] which is orchestrated by the regulation of the pro-apoptotic and anti-apoptotic members of Bcl-2 family including Bad, Bcl-2 and Bcl-XL.[73] For this reason, at early reperfusion we examined the effect of compound **31** on apoptosis markers. We observed an increase in the expression of the antiapoptotic protein Bcl-Xl (*Figure 9E*) which advocates for the alleviation of apoptosis. At this timepoint of reperfusion, we did not observe difference in the expression of Bax (*Figure 9E*) and the protein levels of cleaved caspase 3 were not changed (*Figure 9E*), in accordance with previous reports that demonstrate that cleavage of caspase 3 culminates at 30-60 minutes of reperfusion.[74]

Therefore, the administration of compound **31** preserves ATP and results in cardioprotection through preservation of ATP content, the activation of PKA and RISK signaling (*Figure 10)*.

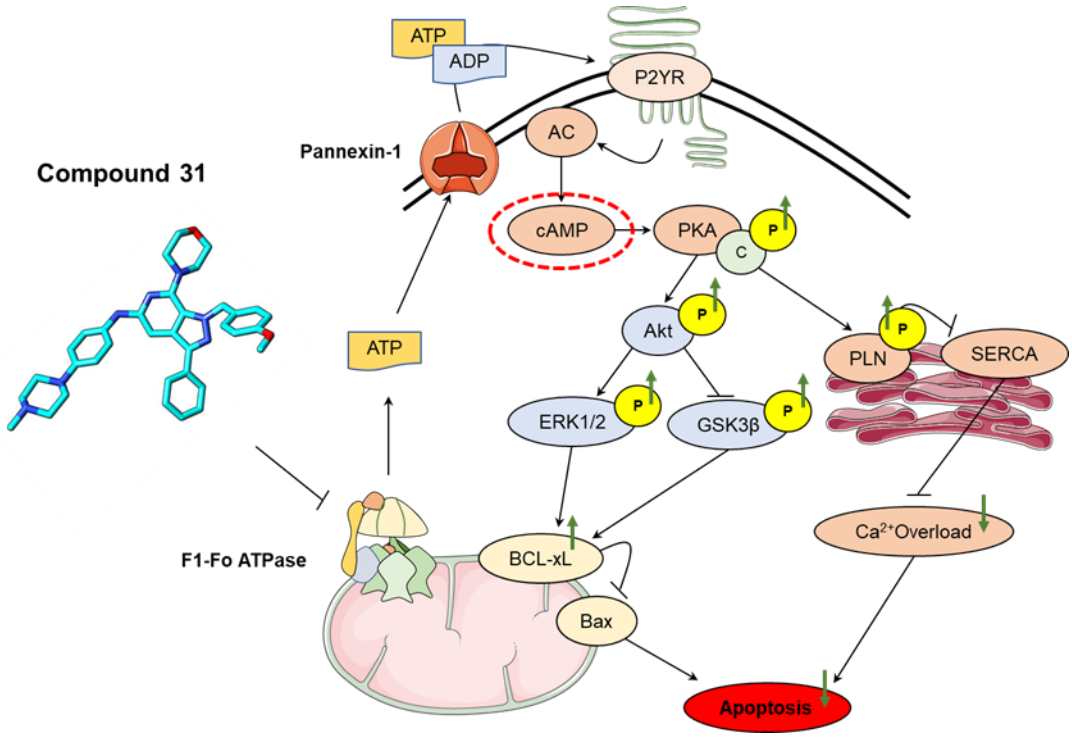

Figure 10: Schematic representation of the cardioprotective mechanism of the ATP hydrolase inhibitor compound 31*. P2YR: purinergic P2Y receptors; AC: adenylyl cyclase; cAMP: cyclic adenosine monophosphate; PKA C-a: Protein kinase A C-alpha; PLN: phospholamban; SERCA: sarco/endoplasmic reticulum Ca^{2+}-ATPase; Akt: protein kinase B; ERK1/2: phospho-p44/p42 MAP kinase, GSK3β: glycogen synthase kinase 3 beta; Bcl-XL: B-cell lymphoma-extra-large; BAX: apoptosis regulator BAX.*

CONCLUSION

The results of the present study highlight that F_1F_O-ATP synthase may serve as a new target for cardioprotection. We identified three pyrazolopyridine analogues which inhibit the ATP hydrolysis without inhibiting ATP synthesis and they also do not interfere with mPTP opening. We present a step by step discovery and hit-to-lead optimization of a novel pyrazolopyridine derivative (**31**) that acts as an inhibitor of ATP hydrolysis targeting the mammalian F_1F_O-ATP synthase with *in vivo* cardioprotective effect against IRI. To the best of our knowledge, this is the first study to evaluate *in vivo* an inhibitor of ATP hydrolysis against cardiac IRI and examine the role of the enzyme at different timepoints with regards to the onset of ischemia. The novel compound **31** significantly reduced myocardial IS when administered prior to and early

during myocardial ischemia. However, compound **31** did not reduce IS when given late during ischemia, before reperfusion. These *in vivo* data taken together suggest that the inhibition of ATP hydrolysis may stand as a cardioprotective target during ischemia and interventions targeting this mechanism should be given as early as possible during the ischemic insult in order to exert their cardioprotective effect. Further studies are necessary to evaluate the effect of the novel ATP hydrolysis inhibitor against IRI in terms of prevention of the onset of heart failure that follows the ischemic insult and also to examine whether sex-specific differences exist for ATP hydrolysis in terms of cardioprotection.

We also provide the first *in vivo* data regarding the activation of the signaling pathways of cardioprotection upon the administration of the new inhibitor of ATP hydrolysis during ischemia. Compound **31** increased the phosphorylation and activation of PKA and PLN which led to IS reduction.[65] Moreover, compound **31** activates the RISK pathway which is an established cardioprotective mechanism that reduces apoptotic signaling and IS.[65] In this study, we proposed that the alleviation of ATP hydrolysis resulted in PKA activation which has the ability to i) integrate receptor and nonreceptor tyrosine kinase signaling into the RISK (Phosphoinositide 3-kinase - PI3K/Akt) pathway[68] and ii) phosphorylate PLN which both pathways may regulate apoptosis (Figure 10). Subsequently we determined the effect of compound **31** on apoptosis signaling molecules. The inhibition of ATP hydrolysis by **31** resulted in the increase of Bcl-XL which prevents apoptosis either by sequestering pro-forms of death-driving cysteine apoptosome proteases (caspases) or by preventing the release of mitochondrial apoptogenic factors such as cytochrome c.[76]

Overall, we herein provide for the first-time *in vivo* data supporting that the inhibition of ATP hydrolysis with a selective small molecule inhibitor could serve as a target for cardioprotection and the basis for testing of F_1F_O-ATP hydrolase inhibitors in cardiovascular disease.

EXPERIMENTAL SECTION

Reagents

In the present study, oligomycin was used as a known potent inhibitor of F_1F_O-ATP synthase.[10] Additionally, BTB06584 which has been previously described as a specific inhibitor of the hydrolytic activity of ATPase was purchased by Cayman Chemicals via Lab Supplies, Galanis, Athens, Greece. All the other reagents were purchased from Sigma Aldrich (via Life Science Chemilab SA and Tech-Line chemicals SA, Athens, Greece), while the antibodies were purchased from Cell Signaling Technology (via Bioline, E. Demagkos & Co, Athens, Greece), unless otherwise stated.

In silico studies

Ligand Preparation

For the ligand-based virtual screening, we utilized our in-house chemical database of 2000 molecules, consisting natural products, synthetic and semi-synthetic compounds together with NCI open database. All ligands were prepared using the ligprep module as implemented on Schrodinger Suite 2021. The final output file was passed through Omega Software (OMEGA 4.2.1.1: OpenEye Scientific Software, Santa Fe, NM. http://www.eyesopen.com.)[77] to generate up to 200 conformers per ligand for further virtual similarity screening.

Similarity search

For similarity search we utilized the ROCS software (ROCS 3.5.1.1: OpenEye Scientific Software, Santa Fe, NM. http://www.eyesopen.com.)[78] with defaults parameters. For each query molecule the whole database was passed through similarity search.

C57BL/6J mice

For the conduction of the study 92 C57BL/6J (WT) male mice 10-14 weeks old (24.7-29.2 g) were used. All animal procedures were performed in compliance with the Presidential Decree 56/2013 for the protection of the animals used for scientific purposes, in harmonization to the European Directive 2010/63 and the experimental protocols were approved by the competent Veterinary Service of the Prefecture of Athens (Protocol number: 471911/06-07-2020). Mice were housed and maintained in a maximum of 6 per cage, in a specific pathogen-free facility at temperature-controlled environment (20-25°C), under a 12-hour light/dark cycle and received regular laboratory animal diet ad libitum. Surgical procedures on the animals and the interventions were performed in compliance with the guidelines "Practical guidelines for rigor and reproducibility in preclinical and clinical studies on cardioprotection"[8,25], i.e. randomization was performed for all the series of experiments and the ischemia/reperfusion surgeries in mice and the calculations of IS were performed by the investigators in a blinded manner.

Isolation of mitochondria from heart tissue

Mitochondria were isolated as previously described from murine hearts.[10,79] The mice were sacrificed through cervical dislocation. The heart was quickly excised and cut in isolation buffer (225 mM mannitol, 75 mM sucrose, 10 mM HEPES-Tris, 1 mM EGTA-Tris, pH 7.4). All the procedures were performed in 4^{o}C with the use of ice. The tissue was homogenized in 0.1mg/mL Nagarse (proteinase type XXIV diluted in isolation buffer) in a glass –Teflon homogenizer. Then, 0.2% w/v of bovine serum albumin (fat acid free) in isolation buffer was added and the homogenate was centrifuged at 500g for 10 min at 4^{o} C. The supernatant was filtered through a 150-mm mesh for the removal of cellular debris. To obtain the mitochondrial pellet, the supernatant was further centrifuged at 8.000g for 10 min at 4^{o} C. The supernatant was decanted; the

mitochondria pellet was re-suspended in isolation buffer and centrifuged once more at 8.000g for 10 min at 4^{o} C. The final pellet was re-suspended in a small volume of isolation buffer (200μL) and was used for protein determination CRC assay.

Investigation of mitochondrial F_1F_O-ATP hydrolase activity in isolated mitochondria

We explored the possible effect of the candidate ATP synthase inhibitors on the ATP-hydrolase activity with a previously described method[80]. Freshly isolated mitochondria from murine hearts (0.25mg) were diluted in ATPase reaction buffer (in mM: Sucrose 125, KCl 65, $MgCl_2$ 2.5 HEPES 50, pH=7.2). For the screening, the mitochondria were treated with 200μM of the compounds and for the determination of the IC_{50} the mitochondria were treated with various concentrations 4000μM, 1000μM, 500μM or 400μM, 200μM, 100μM, 10μM, 1μM and 0.1μM) or DMSO. Oligomycin (10μM) was used as positive control of the assay. The samples were placed in a water bath at 37 ^{o}C and the reaction was initiated by supplementing with 2.5mM of ATP. After incubation for 10 min, the reaction was stopped with trichloroacetic acid (TCA) 40%. Then, molybdate reagent (5 g of ferrous sulfate-FeSO4 in 60 mL of ddH_2O, 10 mL of a 10 % ammonium molybdate -$(NH_4)_6Mo_7O_2.4H_2O$- in 10N H_2SO_4 solution, volume adjustment to 100mL with ddH_2O) was added. After 5 min, the absorbance of the samples was measured at 660nm using the Tecan Infinite 200 PRO series microplate reader (Tecan Group Ltd., Maennedorf, CH). The measurement was performed as an endpoint absobance since the reaction has been stopped with the use of TCA. The calculation of phosphate production using a standard curve (0, 125, 250, 500, 750,1000 nmol Pi) which was generated from a 1mM KH_2PO_4 solution upon subtraction of background signal. Then, the calculation of ATPase activity was performed via the control of the assay that contained DMSO which served as the diluent of the compounds and reached maximum activity. The candidate inhibitors with over 40% inhibition of ATP hydrolysis and the NCI molecules were evaluated using three independent biological

replicates. The IC_{50} values were calculated based on the log(inhibitor) vs. normalized response least squares fit model of GraphPad Prism 8 software (Graph Pad Software, Inc.).

Monitoring the $\Delta\Psi_m$ *in vitro*

H9c2(2-1) cells are a subclone of the original clonal cell line derived from embryonic BD1X rat heart tissue and they are widely used in cardiovascular research.[79] H9c2 cells were grown in standard DMEM (Dulbecco's Modified Eagle's Medium, Catalog No. 30-2002, ATCC) supplemented with FBS (10%), penicillin (100 $U \cdot mL^{-1}$) and streptomycin (100 $\mu g \cdot mL^{-1}$). To assess the different candidate compounds on inhibiting the F_1F_O-ATPase *in vitro*, cells were plated in 96 well-plates (1*10^4 cells/well) and after 24 hours they were treated with 10μM of TMRM in recording buffer for 10 minutes at 37°C. The recording buffer (in mM NaCl 156, KCl, 0.22, $MgSO_4$ 2, K_2HPO_4 1.25, $CaCl_2$ 2, HEPES 10, D-Glucose 10mM, pH=7.4) is a standard imaging solution used to ensure cell viability and mitochondrial metabolism [possibly ref 21 if they used this one?]. The excess extracellular TMRM dye was then washed off. The TMRM rapidly redistributes to the mitochondria, where the high molecular concentration of TMRM quenches its fluorescence signal. The cells were subsequently exposed to rotenone (5 μM), which inhibits complex I of the electron transport chain, resulting in an increase in the reverse, hydrolytic activity of the F_1F_O-ATP synthase, which is sufficient to maintain $\Delta\Psi_m$. Then, the cells were challenged with the candidate inhibitors at several concentrations (10μM, 50μM and 100 μM) to evaluate their ability to inhibit ATP hydrolysis by the F_1F_O-ATP synthase. In the presence of rotenone, inhibition of ATP hydrolysis by the F_1F_O-ATP synthase will negate its ability to maintain the $\Delta\Psi_m$ and thereby results in gradual loss of $\Delta\Psi_m$. $\Delta\Psi_m$ was monitored by the fluorescence of the lipophilic cationic fluorescent TMRM dye measured in the Tecan Infinite 200 PRO series microplate reader. At high (ie micromolar) concentrations of TMRM, when the $\Delta\Psi_m$ falls, the dye, initially located in the mitochondria, rapidly

redistributes to the cytosol in accordance with Nernstian principles, where the relatively larger volume causes it to dequench and hence its fluorescence increases[21][if they need more evidence about this, can add here PMID: 18314743]. The experiment was repeated without the addition of rotenone and any loss of $\Delta\Psi_m$ which was obvious as an increase in the fluorescence was interpreted as cellular toxicity (since it occurred independently of ATPase inhibition). The measurement of fluorescence was performed in a kinetic manner and was measured every 15 seconds for 30 minutes (Ex544/Em590nm). Towards the end of the fluorescence monitoring, the mitochondrial uncoupler carbonyl cyanide-p-trifluoromethoxyphenylhydrazone (FCCP), which causes mitochondrial depolarization was added at a final concentration of 5μM. FCCP results in rapid loss of $\Delta\Psi_m$ that can not be restored by ATP synthase, resulting in rapid redistribution of TMRM to the cytosol and an increase in fluorescence due to dequenching.

Cell viability assay (MTT Assay)

H9c2(2-1) cells were grown in standard DMEM supplemented with FBS (10%), penicillin (100 $U \cdot mL^{-1}$) and streptomycin (100 $\mu g \cdot mL^{-1}$). To assess the viability of the cells upon treatment with the various compounds *in vitro*, cells were plated in 96 well-plates (1*10^4 cells/well) in starvation medium (without FBS) and after 24 hours, they were treated with 100μM , 50μM and 10μM of the tested compounds in recording buffer for 1 hour. After the end of the treatment period, the culture medium was aspirated and 100 uL of fresh medium were added into each 96-well. 10 μL of the MTT reagent (5 mg/mL) were added and mixed with the medium into each 96-well, and cells were incubated into the incubator for 4 hours, until a purple precipitate was visible at the wells' bottom. After the end of the incubation, the MTT medium was aspirated and 100 μL of DMSO were added into each well, in order to dissolve the purple crystal-like formazan MTT product. Finally, absorption was measured at 570 nm and 640 nm using the Tecan Infinite 200 PRO series microplate reader and cell viability was determined

as percentage of the control which was DMSO treated cells (5% of the final volume of the assay).

Calcium retention capacity assay (CRC) in isolated mitochondria

The CRC assay determination in mitochondria was conducted as previously described[10,79] in order to challenge mitochondria with spikes of calcium ions to undergo permeability transition. Isolated mitochondria were diluted in mitochondrial assay buffer (KCl 137 mM, KH_2PO_4 2 mM, HEPES 20 mM, EGTA 20 mM, glutamate/malate 5 mM, pH 7.2) at a concentration of 0.25 mg/ml. Each minute, pulses of 10 mM Ca^{2+} were added to each well and upon opening of the mPTP, Ca^{2+} leaks into the assay buffer and increases fluorescence of the membrane-impermeable CalciumGreen–5N (Molecular Probes) (1μM). Fluorescence was measured using a Fluoroskan Ascent FL plate reader (Thermo Electron, Waltham, MA). Cyclosporine A (CsA) (1 μg/ml) was used as a positive control. Mitochondria were exposed to different concentrations of the candidate ATPase inhibitors and their calcium retention capacity was determined. All experiments were performed in three repetitions.

Chemistry

General information

Melting points were determined on a Büchi apparatus and are uncorrected. ^{1}H-NMR spectra were recorded on a Bruker Avance III 600 or a Bruker Avance DRX 400 instrument, whereas ^{13}C-NMR spectra were recorded on a Bruker Avance III 600 in deuterated solvents and were referenced to TMS (δ scale). The signals of ^{1}H and ^{13}C spectra were unambiguously assigned by using 2D NMR techniques: COSY, NOESY, HMQC and HMBC. Mass spectra were recorded with a LTQ Orbitrap Discovery instrument, possessing an Ionmax ionization source. Flash chromatography was performed on Merck silica gel 60 (0.040-0.063 mm). Analytical thin layer chromatography (TLC) was carried out on precoated (0.25 mm) Merck silica gel F-254

plates. The purity of the target derivatives (>95%) was determined on a Thermo Finnigan® HPLC System (P4000 Pump, AS3000 Autosampler, UV Spectra System UV6000LP detector, Chromquest™ 4.1 Software); Fortis® UniverSil HS-C18 (150 mm, 4.6 mm, 5 µm); mobile phase 1% acetic acid in water/ acetonitrile; flow rate 0.8 mL/min; column temperature 25 °C; injection volume 10 µL.

Detailed experimental conditions for the synthesis

5-Chloro-3-(3-fluorophenyl)-1-methyl-1*H*-pyrazolo[3,4-*c*]pyridine (5)

To a solution of **1** (950 mg, 3.24 mmol) in a mixture of toluene/ethanol/water (80/12/4, 10 ml) were added 3-fluorophenylboronic acid (452 mg, 3.24 mmol), $Pd(PPh_3)_4$ (190 mg, 0.16 mmol) and $NaHCO_3$ (816 mg, 9.71 mmol) and the resulting mixture was heated at 100 ^oC for 30 h. The solvent was then vacuum concentrated, and the residue was extracted with dichloromethane, the organic phase was dried (Na_2SO_4) and concentrated to dryness. The residue was purified by column chromatography (silica gel) using a mixture of dichloromethane / ethyl acetate 98/2 as the eluent to result in 770 mg (87 %) of **5**, as a white solid. Mp. 140-141 ^oC (CH_2Cl_2/Et_2O). ^1H NMR (600 MHz, $CDCl_3$) δ 4.18 (s, 3H, CH_3), 7.15 (m, 1H, fluorophenyl-H4), 7.50 (m, 1H, fluorophenyl-H5), 7.57 (m, 1H, fluorophenyl-H2), 7.63 (m, 1H, fluorophenyl-H6), 7.80 (s, 1H, H-4), 8.64 (s, 1H, H-7).

5-Chloro-3-(3-fluorophenyl)-1-(4-methoxybenzyl)-1*H*-pyrazolo[3,4-*c*]pyridine (6)

This compound was prepared following a method analogous to that of **5**, starting from **2**. Yield 96 %. Mp. 147-149 ^oC (CH_2Cl_2/Et_2O). ^1H NMR (600 MHz, $CDCl_3$) δ 3.78 (s, 3H, OCH_3), 5.64 (s, 2H, CH_2), 6.87 (d, 2H, PMB-H3,5, J=6.9 Hz), 7.14 (m, 1H, fluorophenyl-H4), 7.26 (d, 2H, PMB-H2,6, J=6.9 Hz), 7.49 (m, 1H, fluorophenyl-H5), 7.66 (m, 1H, fluorophenyl-H2), 7.71 (m, 1H, fluorophenyl-H6), 7.88 (s, 1H, H-4), 8.61 (s, 1H, H-7).

5-Chloro-1-methyl-3-phenyl-1*H*-pyrazolo[3,4-*c*]pyridine *N*-oxide (7)

To a solution of **3** (260 mg, 1.06 mmol) in dichloromethane (7 ml) was added 3-chloroperbenzoic acid (70% in water, 615 mg, 3.56 mmol) and the mixture was stirred at rt for 48 h. The solvent was then vacuum-evaporated and the residue was purified by column chromatography (silica gel) using a mixture of cyclohexane / ethyl acetate 7/3 as the eluent to result in **7** (180 mg, 65%) as a white solid. Mp. 219-220 ^{o}C (EtOAc-Et_2O). ^{1}H NMR (400 MHz, $CDCl_3$) δ (ppm) 4.07 (s, 3H, CH_3), 7.43 (t, 1H, 3-phenyl-H4, J=7.1 Hz), 7.50 (t, 2H, 3-phenyl-H3,5, J=7.3 Hz), 7.80 (d, 2H, 3-phenyl-H2,6, J=7.3 Hz), 8.01 (s, 1H, H-4), 8.80 (s, 1H, H-7).

5-Chloro-1-methyl-3-(3-fluorophenyl)-1*H*-pyrazolo[3,4-*c*]pyridine *N*-oxide (9)

This compound was prepared following a method analogous to that of **7**, starting from **5**. Yield 52%. Mp. 247-248 ^{o}C (EtOAc). ^{1}H NMR (600 MHz, $CDCl_3$) δ 4.12 (s, 3H, CH_3), 7.16 (m, 1H, fluorophenyl-H4), 7.50 (m, 1H, fluorophenyl-H5), 7.57 (m, 1H, fluorophenyl-H2), 7.63 (m, 1H, fluorophenyl-H6), 8.08 (s, 1H, H-4), 8.85 (s, 1H, H-7).

5-Chloro-1-(4-methoxybenzyl)-3-(3-fluorophenyl)-1*H*-pyrazolo[3,4-*c*]pyridine *N*-oxide (10)

This compound was prepared following a method analogous to that of **7**, starting from **6**. Yield 48 %. Mp. 200-201^{o}C (CH_2Cl_2). ^{1}H NMR (600 MHz, $CDCl_3$) δ 3.82 (s, 3H, OCH_3), 5.54 (s, 2H, CH_2), 6.91 (d, 2H, PMB-H3,5, J= 6.9 Hz), 7.20 (m, 1H, fluorophenyl-H4), 7.28 (d, 2H, PMB-H2,6, J= 6.9 Hz), 7.54 (m, 1H, fluorophenyl-H5), 7.64 (m, 1H, fluorophenyl-H2), 7.69 (m, 1H, fluorophenyl-H6), 8.08 (s, 1H, H-4), 8.68 (s, 1H, H-7).

5,7-Dichloro-1-methyl-3-phenyl-1*H*-pyrazolo[3,4-*c*]pyridine (11)

To a solution of **7** (160 mg, 0.62 mmol) in dry THF (4.5 ml) was added dropwise under ice-cooling phosphorus oxychloride (0.3 ml, 3.18 mmol) and the mixture was stirred at

rt for 12h. The mixture was then poured into ice-water, made alcaline with the addition of potassium carbonate (pH=10-11) and extracted with ethyl acetate. The organic phase was dried (Na_2SO_4) and concentrated to dryness to provide pure **11** (160 mg, 94%) as a white solid. Mp. 134-135 ^oC (CH_2Cl_2-Et_2O). ^1H NMR (400 MHz, $CDCl_3$) δ 4.42 (s, 3H, CH_3), 7.41 (t, 1H, 3-phenyl-H4, J=7.3 Hz), 7.48 (t, 2H, 3-phenyl-H3,5, J=7.4 Hz), 7.74 (s, 1H, H-4), 7.78 (d, 2H, 3-phenyl-H2,6, J=7.4 Hz). ^{13}C NMR (151 MHz, $CDCl_3$) δ 39.37, 114.43, 127.39, 129.07, 129.30, 130.59, 131.65, 133.09, 134.49, 139.13, 143.57.

5,7-Dichloro-1-methyl-3-(3-fluorophenyl)-1*H*-pyrazolo[3,4-*c*]pyridine (13)

This compound was prepared following a method analogous to that of **11**, starting from **9**. Yield 91%. Mp. 123-125 ^oC (CH_2Cl_2/Et_2O). ^1H NMR (600 MHz, $CDCl_3$) δ 4.47 (s, 3H, CH_3), 7.13 (m, 1H, fluorophenyl-H4), 7.48 (m, 1H, fluorophenyl-H5), 7.56 (m, 1H, fluorophenyl-H2), 7.62 (m, 1H, fluorophenyl-H6), 7.79 (s, 1H, H-4). ^{13}C NMR (151 MHz, $CDCl_3$) δ 39.49, 114.10, 114.14, 114.30, 115.87, 116.01, 122.89, 130.35, 130.85, 130.91, 133.28, 133.69, 133.74, 134.50, 139.46, 142.20, 162.52, 164.16.

5,7-Dichloro-1-(4-methoxybenzyl)-3-(3-fluorophenyl)-1*H*-pyrazolo[3,4-*c*]pyridine (14)

This compound was prepared following a method analogous to that of **11**, starting from **10**. Yield 95%. Mp. 172 ^oC (EtOAc). ^1H NMR (600 MHz, $CDCl_3$) δ 3.76 (s, 3H, OCH_3), 5.96 (s, 2H, CH_2), 6.85 (d, 2H, PMB-H3,5, J= 6.9 Hz), 7.15 (m, 1H, fluorophenyl-H4), 7.25 (d, 2H, PMB-H2,6, J= 6.9 Hz), 7.50 (m, 1H, fluorophenyl-H5), 7.61 (m, 1H, fluorophenyl-H2), 7.66 (m, 1H, fluorophenyl-H6), 7.82 (s, 1H, H-4). ^{13}C NMR (151 MHz, $CDCl_3$) δ 54.33, 55.39, 114.16, 114.31, 114.45, 115.94, 116.08, 123.02, 128.72, 128.84, 130.82, 130.85, 130.88, 132.91, 133.70, 133.76, 133.98, 139.60, 142.89, 159.59, 162.50, 164.14.

5-Chloro-1-methyl-7-(4-methylpiperazin-1-yl)-3-phenyl-1*H*-pyrazolo[3,4-*c*]pyridine (15)

A solution of **11** (80 mg, 0.29 mmol) in *N*-methylpiperazine (0.32 ml, 2.86 mmol) was refluxed for 20 min. Water was added to the solution and it was extracted with ethyl acetate. The organic phase was dried (Na_2SO_4) and concentrated to dryness to provide pure **15** (90 mg, 92%) as a light brown solid. Mp. 110-114 ^oC (Et_2O). ^1H NMR (600 MHz, $CDCl_3$) δ 2.33 (s, 3H, piperazine-CH_3), 2.61 (m, 4H, piperazine-H3,5), 3.31 (m, 4H, piperazine-H2,6), 4.24 (s, 3H, pyrazole-CH_3), 7.34 (t, 1H, 3-phenyl-H4, J=6.9 Hz), 7.40-7.44 (m, 3H, H-4, 3-phenyl-H3,5), 7.78 (d, 2H, 3-phenyl-H2,6, J=8.2 Hz). ^{13}C NMR (151 MHz, $CDCl_3$) δ 38.45, 46.31, 50.87, 54.76, 109.17, 127.29, 128.57, 129.12, 129.95, 131.46, 132.46, 139.02, 144.09, 149.17. HRMS (ESI) m/z: calculated for $C_{18}H_{21}ClN_5$ $[M+H]^+$: 342.1480; found: 342.1469.

5-Chloro-1-methyl-7-(4-methylpiperazin-1-yl)-3-(3-fluorophenyl)-1*H*-pyrazolo[3,4-*c*]pyridine (16)

This compound was prepared following a method analogous to that of **15**, starting from13. Purification by column chromatography (silica gel) using a mixture of dichloromethane / methanol 98/2 as the eluent. Yield 94%. Mp. 140-141 ^oC (CH_2Cl_2/n-pentane). ^1H NMR (600 MHz, $CDCl_3$) δ 2.38 (s, 3H, piperazine-CH_3), 2.65 (m, 4H, piperazine-H3,5), 3.35 (m, 4H, piperazine-H2,6), 4.29 (s, 3H, CH_3), 7.09 (m, 1H, fluorophenyl-H4), 7,45 (m, 1H, fluorophenyl-H5), 7.48 (s, 1H, H-4), 7.52 (m, 1H, fluorophenyl-H2), 7.59 (m, 1H, fluorophenyl-H6). ^{13}C NMR (151 MHz, $CDCl_3$) δ 38.53, 46.27, 50.87, 54.69, 108.75, 113.91, 114.06, 115.26, 115.40, 122.74, 129.69, 130.59, 130.65, 131.41, 134.54, 134.59, 139.29, 142.62, 142.63, 149.22, 162.45, 164.08. HRMS (ESI) m/z: calculated for $C_{18}H_{20}ClFN_5$ $[M+H]^+$: 360.1386; found: 360.1376.

5-Chloro-1-methyl-7-(3-trifluoromethylphenyloxy)-3-phenyl-1*H*-pyrazolo[3,4-*c*]pyridine (17)

To a solution of 3-trifluoromethylphenol (124 mg, 0.76 mmol) in dry DMSO (3 ml) was added at 0 ^{o}C under Ar potassium carbonate (53mg, 0.38mmol) and the mixture was stirred at rt for 30 min. A solution of the dichloride **11** (212 mg, 0.76 mmol) in DMSO (1 mL) was then added and the mixture was heated at 150 ^{o}C for 150 min. Water was added to the mixture and it was extracted with chloroform, the organic phase was washed with brine, dried (Na_2SO_4) and concentrated to dryness. The residue was purified by column chromatography (silica gel) using a mixture of cyclohexane / ethyl acetate 90/10 as the eluent to result in **17** (85 mg, 69%) as a white solid. Mp. 129-131 ^{o}C (Et_2O/n-pentane). ^{1}H NMR (600 MHz, $CDCl_3$) δ 4.42 (s, 3H, pyrazole-CH_3), 7.43 (t, 1H, 3-phenyl-H4, J=7.4 Hz), 7.52 (t, 2H, 3-phenyl-H3,5, J=7.6 Hz), 7.54-7.62 (m, 5H, H-4, 4x 7-phenyloxy-H), 7.88 (d, 2H, 3-phenyl-H2,6, J=7.6 Hz). ^{13}C NMR (151 MHz, $CDCl_3$) δ 39.23, 110.55, 118.75, 121.05, 122.86, 124.86, 126.47, 122.46, 125.14, 127.25, 127.47, 128.75, 129.21, 130.35, 130.88, 132.04, 132.26, 132.48, 132.70, 132.25, 137.29, 143.68, 147.56, 152.76. HRMS (ESI) m/z: calculated for $C_{20}H_{14}ClF_3N_3O$ $[M+H]^+$: 404.0772; found: 404.0758.

5-Chloro-1-methyl-7-(3-trifluoromethylphenyloxy)-3-(3-fluorophenyl)-1*H*-pyrazolo[3,4-*c*]pyridine (18)

This compound was prepared following a method analogous to that of **17**, starting from **13**. Purification by column chromatography (silica gel) using a mixture of cyclohexane / dichloromethane 80/20 as the eluent. Yield 56 %. Mp. 149 ^{o}C (Et_2O). ^{1}H NMR (600 MHz, $CDCl_3$) δ 4.44 (s, 3H, CH_3), 7.12 (m, 1H, fluorophenyl-H4), 7.47 (m, 1H, fluorophenyl-H5), 7.53-7.62 (m, 6H, 4 x7-phenyloxy-H, fluorophenyl-H2, H-4), 7.66 (m, 1H, fluorophenyl-H6). ^{13}C NMR (151 MHz, $CDCl_3$) δ 39.34, 110.18, 113.95, 114.10, 115.49, 115.63, 118.76, 118.78, 121.03, 122.53, 122.54, 122.73, 122.84, 124.65, 125.17, 126.45, 127.47, 130.37, 130.67, 130.74, 130.79, 132.05, 132.26, 132.48, 132.70, 134.35, 134.40, 137.66, 142.31, 147.63, 152.63, 162.55, 164.18. HRMS (ESI) m/z: calculated for $C_{20}H_{13}ClF_4N_3O$ $[M+H]^+$: 422.0678; found: 422.0659.

5-Chloro-1-(4-methoxybenzyl)-7-(4-methylpiperazin-1-yl)-3-(3-fluorophenyl)-1*H*-pyrazolo[3,4-*c*]pyridine (19)

This compound was prepared following a method analogous to that of **15**, starting from **14**. Oil, yield 94%. ^{1}H NMR (600 MHz, $CDCl_3$) δ 2.39 (s, 3H, piperazine-CH_3), 2.66 (m, 4H, piperazine-H3,5), 3.37 (m, 4H, piperazine-H2,6), 3.74 (s, 3H, OCH_3), 5.73 (s, 2H, CH_2), 6.79 (d, 2H, PMB-H3,5, J= 6.8 Hz), 7.09 (m, 1H, fluorophenyl-H4), 7.19 (d, 2H, PMB-H2,6, J= 6.8 Hz), 7.44 (m, 1H, fluorophenyl-H5), 7.48 (s, 1H, H-4), 7.58 (m, 1H, fluorophenyl-H2), 7.63 (m, 1H, fluorophenyl-H6). ^{13}C NMR (151 MHz, $CDCl_3$) *δ* 46.27, 50.63, 53.45, 54.78, 55.33, 109.18, 114.12, 114.14, 114.29, 115.40, 115.54, 122.93, 128.88, 129.10, 130.57, 130.63, 130.80, 130.99, 134.55, 134.61, 139.64, 143.79, 149.16, 159.30, 162.45, 164.08. HRMS (ESI) m/z: calculated for $C_{25}H_{26}ClFN_5O$ $[M+H]^+$: 466.1805; found: 466.1790.

5-Chloro-1-(4-methoxybenzyl)-7-(3-trifluoromethylphenyloxy)-3-phenyl-1*H*-pyrazolo[3,4-*c*]pyridine (20)

This compound was prepared following a method analogous to that of **17**, starting from **12**. Purification by column chromatography (silica gel) using a mixture of cyclohexane / ethyl acetate 90/10 as the eluent. Yield 57%. Mp. 129-131 ºC (Et_2O). ^{1}H NMR (600 MHz, $CDCl_3$) *δ* 3.76 (s, 3H, OCH_3), 5.85 (s, 2H, CH_2), 6.81 (d, 2H, PMB-H3,5, J=8.7 Hz), 7.24 (d, 2H, PMB-H2,6, J=8.7 Hz), 7.37 (brs, 1H, 7-phenyloxy-H2), 7.39-7.42 (m, 1H, 7-phenyloxy-H6), 7.44 (t, 1H, 3-phenyl-H4, J=7.4 Hz), 7.51-7.58 (m, 4H, 3-phenyl-H3,5, 7-phenyloxy-H4,5), 7.60 (s, 1H, H-4), 7.92 (d, 2H, 3-phenyl-H2,6, J=7.6 Hz). ^{13}C NMR (151 MHz, $CDCl_3$) *δ* 55.34, 55.36, 110.53, 114.18, 118.81, 121.02, 122.83, 124.63, 126.44, 122.45, 125.31, 126.76, 127.32, 128.73, 128.96, 129.15, 129.30, 130.34, 131.44, 131.96, 132.18, 132.39, 132.61, 132.30, 137.52, 143.96, 147.46, 152.67, 159.55. HRMS (ESI) m/z: calculated for $C_{27}H_{20}ClF_3N_3O_2$ $[M+H]^+$: 510.1191; found: 510.1179.

5-Chloro-1-(4-methoxybenzyl)-7-(3-trifluoromethylphenyloxy)-3-(3-fluorophenyl)-1*H*-pyrazolo[3,4-*c*]pyridine (21)

This compound was prepared following a method analogous to that of **17**, starting from **14**. Yield 50%. Mp. 148 ^{o}C (EtOAc). ^{1}H NMR (600 MHz, $CDCl_3$) δ 3.78 (s, 3H, OCH_3), 5.87 (s, 2H, CH_2), 6.84 (d, 2H, PMB-H3,5, J= 6.8 Hz), 7.14 (m, 1H, fluorophenyl-H4), 7.25 (d, 2H, PMB-H2,6, J= 6.8 Hz), 7.39 (s, 1H, 7-phenyloxy-H), 7.43 (m, 1H, 7-phenyloxy-H), 7.51 (m, 1H, fluorophenyl-H5), 7.55-7.62 (m, 3H, 2 x 7-phenyloxy-H, H-4), 7.67 (m, 1H, fluorophenyl-H2), 7.72 (m, 1H, fluorophenyl-H6). ^{13}C NMR (151 MHz, $CDCl_3$) δ 55.38, 55.49, 110.22, 114.11, 114.25, 115.54, 115.68, 118.85, 118.87, 121.01, 122.56, 122.58, 122.86, 124.62, 125.35, 126.43, 126.80, 129.04, 129.09, 130.36, 130.72, 130.78, 131.27, 132.03, 132.24, 132.46, 132.68, 134.41, 134.47, 137.93, 142.70, 147.58, 152.58, 159.64, 162.55, 164.18. HRMS (ESI) m/z: calculated for $C_{27}H_{19}ClF_4N_3O_2$ $[M+H]^+$: 528.1097; found: 528.1081.

5-Chloro-1-(4-methoxybenzyl)-7-(morpholin-4-yl)-3-phenyl-1*H*-pyrazolo[3,4-*c*]pyridine (22)

This compound was prepared following a method analogous to that of **15**, starting from **12**. Purification by column chromatography (silica gel) using a mixture of cyclohexane / ethyl acetate 90/10 as the eluent. Oil. Yield 95%. ^{1}H NMR (600 MHz, $CDCl_3$) δ 3.31 (t, 4H, morpholine-H3,5, J=4.5 Hz), 3.71 (s, 3H, OCH_3), 3.91 (t, 4H, morpholine-H2,6, J=4.5 Hz), 5.76 (s, 2H, CH_2), 6.80 (d, 2H, PMB-H3,5, J=8.7 Hz), 7.20 (d, 2H, PMB-H2,6, J=8.7 Hz), 7.39 (t, 1H, 3-phenyl-H4, J=7.4 Hz), 7.48 (t, 2H, 3-phenyl-H3,5, J=7.6 Hz), 7.58 (s, 1H, H-4), 7.89 (d, 2H, 3-phenyl-H2,6, J=7.3 Hz). ^{13}C NMR (151 MHz, $CDCl_3$) δ 51.03, 53.23, 55.10, 66.46, 109.89, 113.96, 127.21, 128.39, 128.51, 128.89, 129.07, 130.85, 132.18, 139.19, 144.85, 148.71, 159.07. HRMS (ESI) m/z: calculated for $C_{24}H_{24}ClN_4O_2$ $[M+H]^+$: 435.1583; found: 435.1574.

5-Chloro-1-(4-methoxybenzyl)-7-(morpholin-4-yl)-3-(3-fluorophenyl)-1*H*-pyrazolo[3,4-*c*]pyridine (23)

This compound was prepared following a method analogous to that of **15**, starting from **14**. Oil. Yield 80%. ^{1}H NMR (600 MHz, $CDCl_3$) δ 3.31 (m, 4H, morpholine-H3,5), 3.73 (s, 3H, OCH_3), 3.92 (m, 4H, morpholine-H2,6), 5.76 (s, 2H, CH_2), 6.80 (d, 2H, PMB-H3,5, J= 6.8 Hz), 7.09 (m, 1H, fluorophenyl-H4), 7.18 (d, 2H, PMB-H2,6, J= 6.8 Hz), 7.44 (m, 1H, fluorophenyl-H5), 7.54 (s, 1H, H-4), 7.60 (m, 1H, fluorophenyl-H2), 7.65 (m, 1H, fluorophenyl-H6). ^{13}C NMR (151 MHz, $CDCl_3$) δ 51.23, 53.55, 55.35, 66.65, 109.77, 114.20, 114.31, 115.49, 115.63, 122.96, 128.62, 129.03, 130.62, 130.68, 130.91, 131.03, 134.45, 134.50, 139.68, 143.82, 148.99, 159.33, 162.47, 164.10. HRMS (ESI) m/z: calculated for $C_{24}H_{23}ClFN_4O_2$ $[M+H]^+$: 453.1489; found: 453.1476.

***N*-[4-(4-methylpiperazin-1-yl)phenyl]-1-methyl-7-(4-methylpiperazin-1-yl)-3-phenyl-1*H*-pyrazolo[3,4-*c*]pyridin-5-amine (24)**

To a solution of **15** (40 mg, 0.12 mmol) in dry toluene (6 ml) were added under Ar 4-(4-methylpiperazin-1-yl)aniline (25 mg, 0.13 mmol), $CsCO_3$ (190 mg, 0.59 mmol), X-Phos (2.77 mg, 0.006 mmol) and $Pd(dba)_2$ (3.34 mg, 0.006 mmol) and the mixture was refluxed for 18 h. Water was then added to the mixture and it was extracted with dichloromethane, the organic phase was dried (Na_2SO_4) and concentrated to dryness. The residue was purified by column chromatography (silica gel) using a mixture of dichloromethane / methanol 95/5 as the eluent to result in **24** (37 mg, 65%), as a white solid. Mp. 216ºC (Acetone). ^{1}H NMR (400 MHz, acetone-d_6) δ 2.25 (s, 3H, piperazine-CH_3), 2.32 (s, 3H, piperazine-CH_3), 2.48 (m, 4H, piperazine-CH_2), 2.64 (m, 4H, piperazine-CH_2), 3.09 (m, 4H, piperazine-CH_2), 3.32 (m, 4H, piperazine-CH_2), 4.28 (s, 3H, pyrazole-CH_3), 6.92 (d, 2H, 5-phenylamino-H2,6, J=8.2 Hz), 6.96 (s, 1H, H-4), 7.35 (t, 1H, 3-phenyl-H4, J=6.6 Hz), 7.41-7.50 (m, 4H, 3-phenyl-H3,5, 5-phenylamino-H3,5), 7.90 (d, 2H, 3-phenyl-H2,6, J=7.4 Hz). ^{13}C NMR (101 MHz, acetone-d_6) δ 38.59, 46.42,

46.46, 50.70, 51.83, 55.69, 56.11, 90.10, 117.82, 120.43, 120.55, 127.32, 128.28, 128.61, 129.58, 131.24, 134.78, 136.48, 136.51, 142.44, 147.02, 147.07, 149.41, 150.20, 150.27. HRMS (ESI) m/z: calculated for $C_{29}H_{37}N_8$ $[M+H]^+$: 497.3136; found: 497.3123.

_N_-[4-(4-methylpiperazin-1-yl)phenyl]-1-methyl-7-(4-methylpiperazin-1-yl)-3-(3-fluorophenyl)-1_H_-pyrazolo[3,4-_c_]pyridin-5-amine (25)

This compound was prepared following a method analogous to that of **24**, starting from **16**. Purification by column chromatography (silica gel) using a mixture of dichloromethane / methanol 95/5 as the eluent. Oil. Yield 65%. ^{1}H NMR (600 MHz, $CDCl_3$) δ 2.38 (s, 3H, piperazine-CH_3), 2.41 (s, 3H, piperazine-CH_3), 2.61-2.73 (m, 8H, anilinopiperazine-H3,5, pyridinopiperazine-H3,5), 3.20 (m, 4H, anilinopiperazine-H2,6), 3.36 (m, 4H, pyridinopiperazine-H2,6), 4.27 (s, 3H, CH_3), 6.14 (brs, 1H, NH, D_2O exch.), 6.85 (s, 1H, H-4), 6.93 (d, 2H, 5-phenylamino-H3,5, J= 6.9 Hz), 7.02 (m, 1H, fluorophenyl-H4), 7.23 (d, 2H, 5-phenylamino-H2,6, J= 6.9 Hz), 7.40 (m, 1H, fluorophenyl-H5), 7.54 (m, 1H, fluorophenyl-H2), 7.58 (m, 1H, fluorophenyl-H6). ^{13}C NMR (151 MHz, $CDCl_3$) δ 38.32, 46.15, 46.32, 49.95, 50.79, 54.97, 55.29, 88.65, 113.64, 113.79, 114.49, 114.63, 117.67, 121.30, 122.50, 128.40, 130.41, 130.47, 130.51, 134.85, 135.69, 135.74, 141.69, 146.82, 148.76, 149.22, 162.47, 164.10. HRMS (ESI) m/z: calculated for $C_{29}H_{36}FN_8$ $[M+H]^+$: 515.3041; found: 515.3021.

_N_-[4-(4-methylpiperazin-1-yl)phenyl]-1-methyl-7-(3-trifluoromethylphenyloxy)-3-phenyl-1_H_-pyrazolo[3,4-_c_]pyridin-5-amine (26)

This compound was prepared following a method analogous to that of **24**, starting from **17**. Purification by column chromatography (silica gel) using a mixture of dichloromethane / methanol 95/5 as the eluent. Mp. 168-169 ^{o}C (Et_2O). Yield 64%. ^{1}H NMR (600 MHz, acetone-d_6) δ 2.25 (s, 3H, piperazine-CH_3), 2.47 (m, 4H, piperazine-H3,5), 3.03 (m, 4H, piperazine-H2,4), 4.38 (s, 3H, CH_3), 6.72 (d, 2H, 5-phenylamino-

H2,6, J=6.3 Hz), 7.00 (s, 1H, H-4), 7.12 (d, 2H, 5-phenylamino-H3,5, J=8.6 Hz), 7.37 (t, 1H, 3-phenyl-H4, J=6.9 Hz), 7.49 (t, 2H, 3-phenyl-H3,5, J=7.5 Hz), 7.56 (brs, 1H, D_2O exch, NH), 7.69-7.74 (m, 2H, 7-phenyloxy-H5,6), 7.75-7.80 (m, 2H, 7-phenyloxy-H2,4), 7.93 (d, 2H, 3-phenyl-H2,6, J=7.3 Hz). ^{13}C NMR (151 MHz, acetone-d_6) δ 39.22, 46.42, 50.68, 56.09, 90.59, 117.62, 120.34, 120.47, 122.74, 124.14, 124.23, 125.94, 127.31, 127.52, 128.44, 129.66, 131.60, 132.26, 132.48, 132.64, 134.62, 135.85, 135.88, 142.01, 147.12, 147.17, 148.75, 149.39, 149.47, 154.86. HRMS (ESI) m/z: calculated for $C_{31}H_{30}F_3N_6O$ $[M+H]^+$: 559.2428; found: 559.2415.

_N_-[4-(4-methylpiperazin-1-yl)phenyl]-1-methyl-7-(3-trifluoromethylphenyloxy)-3-(3-fluorophenyl)-1_H_-pyrazolo[3,4-_c_]pyridin-5-amine (27)

This compound was prepared following a method analogous to that of **24**, starting from **18**. Oil. Yield 20%. ^1H NMR (600 MHz, $CDCl_3$) δ 2.38 (s, 3H, piperazine-CH_3), 2.62 (m, 4H, piperazine-H3,5), 3.17 (m, 4H, piperazine-H2,6), 4.38 (s, 3H, CH_3), 5.96 (brs, 1H, NH, D_2O exch.), 6.84-6.87 (m, 3H, 5-phenylamino-H2,4, H-4), 7.01-7.12 (m, 3H, fluorophenyl-H4, 5-phenylamino-H3,5), 7.42 (m, 1H, fluorophenyl-H5), 7.48-7.62 (m, 6H, 4x7-phenyloxy-H, fluorophenyl-H2, fluorophenyl-H6). ^{13}C NMR (151 MHz, $CDCl_3$) δ 39.11, 46.07, 49.77, 55.21, 88.80, 113.60, 113.76, 114.61, 114.75, 117.57, 119.30, 121.53, 122.08, 122.42, 122.94, 124.08, 124.75, 125.68, 130.23, 130.50, 130.56, 131.84, 131.93, 132.14, 132.36, 132.58, 134.08, 135.54, 135.59, 141.03, 147.06, 147.86, 148.47, 153.29, 162.51, 164.14. HRMS (ESI) m/z: calculated for $C_{31}H_{29}F_4N_6O$ $[M+H]^+$: 577.2333; found: 577.2312.

_N_-[4-(4-methylpiperazin-1-yl)phenyl]-1-(4-methoxybenzyl)-7-(4-methylpiperazin-1-yl)-3-(3-fluorophenyl)-1_H_-pyrazolo[3,4-_c_]pyridin-5-amine (28)

This compound was prepared following a method analogous to that of **24**, starting from **19**. Oil. Yield 48%. ^1H NMR (600 MHz, $CDCl_3$) δ 2.36 (s, 3H, anilinopiperazine-CH_3), 2.40 (s, 3H, pyridinopiperazine-CH_3), 2.60 (m, 4H, anilinopiperazine-H3,5), 2.67 (m,

4H, pyridinopiperazine-H3,5), 3.18 (m, 4H, anilinopiperazine-H2,6), 3.33 (m, 4H, pyridinopiperazine-H2,6), 3.74 (s, 3H, OCH_3), 5.68 (s, 2H, CH_2), 6.18 (brs, 1H, NH, D_2O exch.), 6.78 (d, 2H, PMB-H3,5, J= 6.8 Hz), 6.86 (s, 1H, H-4), 6.93 (d, 2H, 5-phenylamino-H2,6, J= 6.9 Hz), 7.02 (m, 1H, fluorophenyl-H4), 7.21 (d, 2H, PMB-H2,6, J= 6.8 Hz), 7.24 (d, 2H, 5-phenylamino-H2,6, J= 6.9 Hz), 7.38 (m, 1H, fluorophenyl-H5), 7.56 (m, 1H, fluorophenyl-H2), 7.59 (m, 1H, fluorophenyl-H6). ^{13}C NMR (151 MHz, $CDCl_3$) δ 46.22, 46.36, 49.98, 50.63, 53.24, 55.12, 55.32, 89.07, 113.80, 113.97, 114.56, 114.70, 117.54, 121.39, 122.64, 127.77, 128.87, 129.86, 130.33, 130.38, 131.58, 134.64, 135.69, 135.74, 142.84, 146.93, 148.69, 149.56, 159.08, 162.40, 164.03. HRMS (ESI) m/z: calculated for $C_{36}H_{42}FN_8O$ $[M+H]^+$: 621.3460; found: 621.3442.

_N_-[4-(4-methylpiperazin-1-yl)phenyl]-1-(4-methoxybenzyl)-7-(3-trifluoromethylphenyloxy)-3-phenyl-1_H_-pyrazolo[3,4-_c_]pyridin-5-amine (29)

This compound was prepared following a method analogous to that of **24**, starting from **20**. Purification by column chromatography (silica gel) using a mixture of chloroform / methanol 10/0.2 as the eluent. M.p. 155-156 ^{o}C (Et_2O/petroleum ether). Yield 39%. ^{1}H NMR (600 MHz, acetone-d_6) δ 2.25 (s, 3H, piperazine-CH_3), 2.47 (m, 4H, piperazine-H3,5), 3.03 (m, 4H, piperazine-H2,4), 3.74 (s, 3H, OCH_3), 5.85 (s, 2H, CH_2), 6.71 (d, 2H, PMB-H3,5, J=8.7 Hz), 6.87 (d, 2H, 5-phenylamino-H2,6, J=8.8 Hz), 7.01 (s, 1H, H-4), 7.11 (d, 2H, 5-phenylamino-H3,5, J=8.8 Hz), 7.34 (d, 2H, PMB-H2,6, J=8.7 Hz), 7.39 (t, 1H, 3-phenyl-H4, J=7.3 Hz), 7.50 (t, 2H, 3-phenyl-H3,5, J=8.0 Hz), 7.58-7.60 (m, 2H, 7-phenyloxy-H4,6), 7.70 (m, 1H, 7-phenyloxy-H2), 7.75 (m, 1H, 7-phenyloxy-H5), 7.96 (d, 2H, 3-phenyl-H2,6, J=7.7 Hz). ^{13}C NMR (151 MHz, acetone-d_6) δ 46.41, 50.64, 55.49, 55.52, 56.08, 90.76, 114.80, 117.59, 120.24, 120.40, 120.54, 122.78, 123.44, 127.46, 128.60, 129.69, 129.77, 131.09, 131.62, 132.24, 132.46, 133.26, 134.52, 135.75, 142.77, 147.17, 148.47, 149.62, 149.70, 154.71, 160.36. HRMS (ESI) m/z: calculated for $C_{38}H_{36}F_3N_6O_2$ $[M+H]^+$: 665.2846; found: 665.2816.

_N_-[4-(4-methylpiperazin-1-yl)phenyl]-1-(4-methoxybenzyl)-7-(3-trifluoromethylphenyloxy)-3-(3-fluorophenyl)-1_H_-pyrazolo[3,4-_c_]pyridin-5-amine (30)

This compound was prepared following a method analogous to that of **24**, starting from **21**. Oil. Yield 72%. ^{1}H NMR (600 MHz, $CDCl_3$) δ 2.36 (s, 3H, CH_3), 2.59 (m, 4H, piperazine-H3,5), 3.16 (m, 4H, piperazine-H2,6), 3.76 (s, 3H, OCH_3), 5.79 (s, 2H, CH_2), 5.96 (brs, 1H, NH, D_2O exch.), 6.80-6.86 (m, 5H, H-4, PMB-H3,5, 5-phenylamino-H2,6), 7.03-7.09 (m, 3H, 5-phenylamino-H3,5, fluorophenyl-H4), 7.25 (d, 2H, PMB-H2,6, J= 6.8 Hz), 7.35-7.44 (m, 3H, 2 x 7-phenyloxy-H, fluorophenyl-H5), 7.52-7.55 (m, 2H, 7-phenyloxy-H), 7.60-7.66 (m, 2H, fluorophenyl-H2, fluorophenyl-H6). ^{13}C NMR (151 MHz, $CDCl_3$) δ 46.23, 49.88, 55.18, 55.30, 55.35, 88.80, 113.71, 113.86, 114.09, 114.62, 114.76, 117.39, 119.31, 121.10, 121.63, 122.01, 122.51, 122.91, 123.24, 124.72, 125.79, 128.96, 129.80, 130.16, 130.44, 130.50, 132.07, 132.29, 132.45, 133.83, 135.59, 135.64, 141.42, 147.23, 147.72, 148.73, 153.23, 159.41, 162.48, 164.11. HRMS (ESI) m/z: calculated for $C_{38}H_{35}F_4N_6O_2$ $[M+H]^+$: 683.2752; found: 683.2726.

_N_-[4-(4-methylpiperazin-1-yl)phenyl]-1-(4-methoxybenzyl)-7-(morpholin-4-yl)-3-phenyl-1_H_-pyrazolo[3,4-_c_]pyridin-5-amine (31)

This compound was prepared following a method analogous to that of **24**, starting from **22**. Purification by column chromatography (silica gel) using a mixture of dichloromethane / methanol 95/5 as the eluent. Yellow solid. Mp. 203-204ºC (acetone). Yield 53%. ^{1}H NMR (600 MHz, $CDCl_3$) δ 2.38 (s, 3H, CH_3), 2.62 (m, 4H, piperazine-H3,5), 3.19 (m, 4H, piperazine-H2,6), 3.28 (m, 4H, morpholine-H3,5), 3.74 (s, 3H, OCH_3), 3.92 (m, 4H, morpholine-H2,6), 5.71 (s, 2H, CH_2), 6.17 (brs, 1H, D_2O exch, NH), 6.78 (d, 2H, PMB-H3,5, J=8.7 Hz), 6.92-6.95 (m, 3H, H-4, 5-phenylamino-H2,6), 7.19 (d, 2H, 5-phenylamino-H3,5, J=8.7 Hz), 7.23 (d, 2H, PMB-H2,6, J=8.8 Hz), 7.35

(t, 1H, 3-phenyl-H4, J=7.4 Hz), 7.44 (t, 2H, 3-phenyl-H3,5, J=7.5 Hz), 7.84 (d, 2H, 3-phenyl-H-2,6, J=7.4 Hz). ^{13}C NMR (151 MHz, $CDCl_3$) δ 46.06, 49.84, 51.15, 53.23, 55.23, 55.31, 66.92, 89.92, 113.97, 117.65, 121.39, 127.16, 127.79, 127.93, 128.58, 128.90, 129.97, 131.89, 133.41, 134.78, 144.19, 146.78, 148.33, 149.36, 159.03. HRMS (ESI) m/z: calculated for $C_{35}H_{40}N_7O_2$ $[M+H]^+$: 590.3238; found: 590.3213.

_N_-[4-(4-methylpiperazin-1-yl)phenyl]-1-(4-methoxybenzyl)-7-(morpholin-4-yl)-3-(3-fluorophenyl)-1_H_-pyrazolo[3,4-_c_]pyridin-5-amine (32)

This compound was prepared following a method analogous to that of **24**, starting from **23**. Oil. Yield 75%. ^{1}H NMR (600 MHz, $CDCl_3$) δ 2.37 (s, 3H, CH_3), 2.60 (m, 4H, piperazine-H3,5), 3.19 (m, 4H, piperazine-H2,6), 3.28 (m, 2H, morpholine-H3,5), 3.74 (s, 3H, OCH_3), 3.92 (m, 2H, morpholine-H2,6), 5.70 (s, 2H, CH_2), 6.18 (brs, 1H, NH, D_2O exch.), 6.79 (d, 2H, PMB-H3,5, J= 6.8 Hz), 6.90 (s, 1H, H-4), 6.94 (d, 2H, 5-phenylamino-H2,6, J= 6.9 Hz), 7.03 (m, 1H, fluorophenyl-H4), 7.19 (d, 2H, PMB-H2,6, J= 6.8 Hz), 7.23 (d, 2H, 5-phenylamino-H3,5, J= 6.9 Hz), 7.39 (m, 1H, fluorophenyl-H5), 7.57 (m, 1H, fluorophenyl-H2), 7.60 (m, 1H, fluorophenyl-H6). ^{13}C NMR (151 MHz, $CDCl_3$) δ 46.25, 49.96, 51.20, 53.35, 55.34, 66.90, 89.40, 113.82, 113.97, 114.04, 114.64, 114.78, 117.52, 121.58, 122.64, 127.75, 128.62, 129.78, 130.37, 130.42, 131.73, 134.43, 135.60, 135.65, 142.85, 147.12, 148.46, 149.70, 159.12, 162.42, 164.05. HRMS (ESI) m/z: calculated for $C_{35}H_{39}FN_7O_2$ $[M+H]^+$: 608.3144; found: 608.3124.

Protein Preparation

The homology model of ATPase synthase was build using PDB entries 2XND[81,82] as shown on *Supporting Information Table S6*. Every chain was built separately, and the combined final model was further prepared for the docking calculations using the Protein Preparation Workflow (Schrödinger Suite 2021 Protein Preparation Wizard)

implemented in the Schrödinger suite and accessible from within the Maestro program (Maestro, version 12.8, Schrödinger, LLC, New York, NY, USA, 2021). Ligand preparation for docking was performed with the LigPrep application (LigPrep, Schrödinger LLC).

Docking Simulations

The induced-fit docking algorithm was utilized for molecular docking as implemented on Schrödinger Suite 2021 (Schrödinger Release 2021-1: Induced Fit Docking protocol; Glide, Schrödinger, LLC, New York, NY, 2021; Prime, Schrödinger, LLC, New York, NY, 2021). For calculating the grid box size, the center of the grid box was taken to be the center of the ligand in the crystal structure, and the length of the grid box for the receptor was twice the distance from the ligand center to its farthest ligand atom plus 10 Å in each dimension. The scoring calculations were performed using standard precision (SP).

MM-GBSA prediction

Theoretical ΔG MM-GBSA of binding was calculated with the assistance of prime MM-GBSA algorithm as implemented on Schrodinger Suite 2021. The water solvation model of VSGB (variable-dielectric generalized Born model) was utilized and the OPLS_2005 force field as implemented on Schrodinger Suite 2021. We utilized the sampling method of minimization, while all residues within 4.0 Å from the ligand were free to move.

Murine model of ischemia reperfusion and IS determination

Mice were randomized and anesthetized with an intraperitoneal injection of a combination of ketamine (100mg/kg), xylazine (20 mg/kg), and atropine (0.6 mg/kg). The anesthesia depth was monitored by the loss of the pedal reflex. The body temperature was maintained at 37^{o}C throughout the surgical procedure with the use

of a heating pad. Upon performing a tracheotomy, artificial respiration was achieved by a rodent ventilator at a rate of 200 strokes/min and with tidal volume of 0.18 mL. The chest was opened via left-sided thoracotomy and pericardiotomy was performed to visualize the heart. The left anterior descending coronary (LAD) was ligated approximately 3-4 mm distal to the origin of the artery under the left atrium using a 6-0 silk suture and the heart was allowed to stabilize for 15 minutes. After the ischemic period, the ligature was released and allowed reperfusion of the myocardium for 2 hours, as previously described[60,79]. Mice hearts were gently removed, and the aorta was cannulated and perfused with 10mL Krebs buffer. Subsequently, 2% of Evans Blue in Krebs buffer was slowly injected to enable the delineation of the ischemic from non-ischemic zone. The hearts were cut in 1 mm sections and incubated with 1% triphenyl tetrazolium chloride (TTC) at 37 °C for 10 min. so that the infarct area is demarcated as a white area while viable tissue stains red. Subsequently, the slices were photographed with a Cannon Powershot A620 Digital Camera (Canon,Tokyo, Japan) under the Zeiss 459300 microscope (Carl Zeiss Light Microscopy, Göttingen, Germany). The overall size of the each slice (All/A), the area-at-risk (R) and the infarct area (I) were determined using ImageJ software and the percentages of R/A% and I/R % were calculated as described[25,75].

Experimental protocols in vivo

In the first series of experiments twenty five mice were randomized into five groups (n=5 per group): 1) *Control:* Treated with Vehicle (normal saline with 1% Tween 80); 2) *BTB* : BTB was given at a dose of 5 mg/kg; 3) *1117*: compound **1117** was given at 3.6mg/kg, 4) *1119*: compound **1119** was given at 3.5mg/kg and 5) *31*: compound **31** was given at 3.5mg/kg. The compounds were diluted in normal saline with 1% Tween 80 as we have previously described[10]. The interventions were performed intravenously through the jugular vein at the 5 minutes before ischemia. The doses were calculated so that the compounds reach the concentration in the plasma of the mice that was

effective in the *in vitro* assays which is the 100μM for BTB and 50μM for **1117**,**1119** and **31.** At the end of reperfusion IS was determined (*Figure 8A*).

In a second series of experiments, twenty additional mice were randomized into four groups (n=5 per group): 1) *Control*: treated with Vehicle, 2) *31*: that received compound **31** at a dose of 3.5mg/kg and the interventions were performed intravenously through the jugular vein at the 5th minute of ischemia, 3) *Control*: treated with Vehicle and 4) *31*: that received compound **31** at a dose of 3.5mg/kg and the interventions were performed intravenously through the jugular vein at the 25th minute of ischemia. After 30 minutes of ischemia and two hours of reperfusion the infarct size was determined (*Figure 8D*).

In the third series of experiments, we repeated the experimental protocol in which the administrations were performed at the 5th minute of ischemia. We included twelve additional mice (n =6 per group) that underwent 30 minutes ischemia and 10 minutes of reperfusion. At this point, tissue sampling from the ischemic and non-ischemic myocardium in liquid nitrogen was obtained for the measurement of ATP content and Western blot analysis was performed in the ischemic part of the myocardium as we have previously described.[10,77] (*Figure 9A*).

Measurement of ATP content in the myocardium

The ischemic and non-ischemic part of the myocardium for every animal was collected form the animal at the 10th min of reperfusion. 10mg of pulverized tissue were used per sample and were possessed according to manufacturer's instructions for high metabolically active tissues (Abcam, ATP Assay Kit (Colorimetric/Fluorometric) #ab83355). The tissue was homogenized in100μL ice cold 2N Perchloric acid (PCA) with a Dounce homogenizer sitting on ice, with 10-15 passes. The samples were kept on ice for 30-45 minutes and were centrifuged at 13,000 g for 2 minutes at 4°C and the supernatant was transferred to a fresh tube while its volume was simultaneously measured. The supernatant was diluted to 500μL with the Assay Buffer XXIII/ATP

Assay Buffer provided by the kit. Then, the excess PCA was precipitated by adding 75μL of ice-cold 2M KOH and in this way the samples were neutralized. The pH was tested with the use of pH paper test and a pH equal to 6.5-8 was acceptable of further adjusted with 0.1 M KOH or PCA. The samples were centrifuged at 13,000 g for 15 minutes at 4°C and the supernatant was collected. To calculate the dilution factor introduced by the deproteinization step we applied the following formula:

$$DDF = \frac{500\,\mu L + volume\ KOH\ (\mu L)}{initial\ sample\ volume\ in\ PCA\ (100\mu L)}$$

After this step, 30μL of each sample was used for the assay and the same amount was used as sample background control well and diluted to 50 μL of ATP assay buffer according the manufacturer's instructions. Upon completing the assay, the output was measured on the microplate reader Tecan Infinite 200 PRO series at Excitation/ Emission=535/587 nm. The content of the samples in ATP (nmol/μL) was calculated based on the standard curve of ATP with linear regression upon correction for the background and the application of the dilution factors.

Western Blot analysis in myocardial tissue

Western Blot analysis in myocardial tissue samples was performed as previously described[10,47,77]. At the 10th minute of reperfusion period, tissue samples from the ischemic myocardium were snap frozen in liquid nitrogen and subsequently pulverized in dry ice. The powders were homogenized using lysis solution (1% Triton X100, 20 mM Tris pH 7.4–7.6, 150mM NaCl, 50mM NaF, 1mM EDTA, 1mM ethylene glycol tetraacetic acid, 1mM glycerolphosphatase, 1% sodium dodecyl sulfate (SDS), 100mM phenylmethanesulfonyl fluoride, and 0.1% protease phosphatase inhibitor cocktail). Protein content was determined using Lowry method. An equal amount of protein was loaded in each well and then separated by SDS-polyacrylamide gel electrophoresis 6–15% and transferred onto a polyvinylidene difluoride membrane (PVDF). After blocking

with 5% nonfat dry milk, membranes were incubated overnight at 4 °C with the following primary antibodies: phospho-protein kinase A C-alpha (T197, PKA C-a) (dilution 1:1000, Rabbit mAb #4781), PKA C-a (dilution 1:1000, Rabbit mAb #4782), phospho-phospholamban (Ser16/Thr17, p-PLN) (dilution 1:1000, Rabbit mAb #8496), PLN (dilution 1:2000, Rabbit mAb #14562), Ryanodine (dilution 1:2000, mouse sc-376507, Santa Cruz Biotechnology), sarco/endoplasmic reticulum Ca2+-ATPase (SERCA) (dilution 1:1000, Rabbit mAb #4219), troponin-I (TnI) (dilution 1:1000, Rabbit mAb #13083), phospho-protein kinase B (p-Akt) (S473) (dilution 1:1000, Rabbit mAb #4060), Akt (dilution 1:1000, Rabbit mAb #4691), phospho-p44/p42 MAP kinase (T202/Y204, p44/p42 ERK) (dilution 1:1000, Rabbit mAb #9101), p44/p42 ERK (dilution 1:1000, Rabbit mAb #9102), phospho-glycogen synthase kinase 3 beta (S9, GSK3-β) (dilution 1:1000, Rabbit mAb #9323), GSK3β (dilution 1:1000, Rabbit mAb #9315), B-cell lymphoma-extra-large (Bcl-XL) (dilution 1:1000, Rabbit mAb #2764), apoptosis regulator BAX (BAX), (dilution 1:1000, Rabbit mAb #5023), cleaved caspase-3 (Cl. Casp 3) (dilution 1:500, Rabbit mAb #9661), α-actinin (dilution 1:2000, Rabbit mAb #6487). All antibodies were purchased from Cell Signaling Technology unless otherwise stated. Membranes were then incubated with secondary antibodies for 2 h at room temperature (Biorad (goat anti-mouse (#7076) and goat anti-rabbit HRP (#7074)) and developed using the GE Healthcare ECL Western Blotting Detection Reagents (Thermo Scientific Technologies, Thermo Fisher Scientific Inc., Waltham). Relative densitometry was determined and the values for phospho-proteins and were normalized to the values for total respective proteins A-actinin was used as loading control.

Statistical analysis

Values are presented as mean± SD for *in vitro* assays while the *in vivo* data ± standard error (S.E.M) was applied. For *in vitro* and *in vivo* studies where multiple comparisons were needed, One way Analysis of Variance model (ANOVA), followed by Tukey's

multiple comparison test was used. For the effect of compound **31** *in vivo,* the analysis of the ATP content was performed with ANOVA, followed by Tukey's multiple comparison test. The densitometric analysis for Western blots, where comparisons between two groups were needed, an unpaired t test was performed to compare the two groups. A $p < 0.05$ was considered to be statistically significant. Statistical significances were classified as *P<0.05; **P<0.01; ***P<0.001;****P<0.0001. All statistical analyses were carried out using GraphPad Prism version 8 (Graph Pad Software, Inc.)

ASSOCIATED CONTENT

Supporting information: Additional figures illustrating the overview of the experimental protocol, fluorescent tracing and compound **31** binding mode compared to quercetin, Tables with inhibition data of all tested compounds, NMR spectra and HPLC chromatograms. PDB files of the homology modeling and docking calculations. The data generated in this study are provided in the Supplementary Information file and any additional information can be requested from the corresponding author.

AUTHOR INFORMATION

Corresponding Authors

***I.A.: Email :** jandread@pharm.uoa.gr , Phone, +30 210 7274827,

*E.M : Email : mikros@pharm.uoa.gr.:, Phone, +302107274813.

Author contributions

All authors participated in the scientific discussion. I.A. conceived the research. I.A., E.M., S.M.D., P.E.N., P.M. and N.P. designed the experiments. P.E.N. carried out the *in vitro* and *in vivo* experiments, performed the statistical analysis and created the respective figures. P.B.L and K.F assisted in the isolation of mitochondria and the

experiments on H9$_C$2 cells. M.G., S.K., V.K. and N.L. designed, synthesized and characterized the newly synthesized molecules. G.L. and D.K. performed the *in silico* experiments. P.E. performed the Western blot analysis. P.E.N., G.L. and N.L. analyzed the data and discussed the results. P.E.N., G.L. and N.L. wrote the manuscript. I.A., E.M., S.M.D., N.P., P.M. and N.L. revised the manuscript. All authors commented on the manuscript. I.A. supervised the project.

Notes

The authors declare no competing interests. The authors have not received any funding for the conduction of this project.

ACKNOWLEDGEMENTS

This work has been supported in the context of the EU-CARDIOPROTECTION COST-Action (CA16225).

S.M.D would like to acknowledge the British Heart Foundation for the research grants PG/19/51/34493 and PG/16/85/32471.

Figures 1, 3 and 10 were created with the use of graphics provided by Servier Medical Smart Art. Figures 4 and TOC were created with “BioRender.com”.

ABBREVIATIONS USED

AMI, Acute Myocardial Infarction; ANOVA, Analysis of Variance model; ADP, Adenosine diphosphate; Akt: Protein kinase B; ATP, Adenosine triphosphate; BAX, Apoptosis regulator BAX; Bcl-XL, B-cell lymphoma-extra-large; BTB, BTB06584; Cl. Casp 3, cleaved caspase-3; CH_2Cl_2, Dichloromethane; CRC, Calcium Retention Capacity; CsA, Cyclosporin A; $CsCO_3$, Caesium carbonate; DMSO, Dimethyl sulfoxide; EGTA, Ethylene glycol tetraacetic acid; ERK: p44/p42 MAP kinase; EtOH, Ethanol; GSK3β, Glycogen synthase kinase 3 beta; HAX1, HS-1 associated protein X-1; H_2O, Water:, IF_1, inhibitor protein of F1 subunit; IFD, Induced-Fit Docking; IRI,

Ischemia/reperfusion injury; IS,Infarct Size; KCl: Potassium chloride; KH_2PO_4, Potassium dihydrogen phosphate; $MgCl_2$, Magnesium chloride; mPTP, Mitochondrial permeability transition pore; MTT, 3-(4,5-dimethylthiazol-2-yl)-2,5-diphenyl-2H-tetrazolium bromide; ($NaHCO_3$,Sodium bicarbonate; NCI, National Cancer Institute; PCA, Perchloric acid; PDB, Protein Data Bank; $Pd(dba)_2$, Bis(dibenzylideneacetone) palladium; $Pd(PPh_3)_4$, Tetrakis(triphenylphosphine)palladium; PKA, Protein kinase A; PLN, Phospholamban; $POCl_3$, Phosphoryl chloride; SD, Standard deviation; SEM, Standard error; SERCA, Sarcoplasmic reticulum Ca(2+)-ATPase; TMRM, tetramethylrhodamine; TSPO, Translocator protein; TTC, Triphenyltetrazolium chloride; THF, tetrahydrofuran; X-Phos, 2-Dicyclohexylphosphino-2′,4′,6′-triisopropylbiphenyl;

REFERENCES

(1) Chatzianastasiou, A.; Bibli, S.-I.; Andreadou, I.; Efentakis, P.; Kaludercic, N.; Wood, M. E.; Whiteman, M.; Lisa, F. D.; Daiber, A.; Manolopoulos, V. G.; Szabó, C.; Papapetropoulos, A. Cardioprotection by H2S Donors: Nitric Oxide-Dependent and -Independent Mechanisms. *J Pharmacol Exp Ther* **2016**, *358* (3), 431–440. https://doi.org/10.1124/jpet.116.235119.

(2) Zuurbier, C. J.; Bertrand, L.; Beauloye, C. R.; Andreadou, I.; Ruiz-Meana, M.; Jespersen, N. R.; Kula-Alwar, D.; Prag, H. A.; Eric Botker, H.; Dambrova, M.; Montessuit, C.; Kaambre, T.; Liepinsh, E.; Brookes, P. S.; Krieg, T. Cardiac Metabolism as a Driver and Therapeutic Target of Myocardial Infarction. *J Cell Mol Med* **2020**, *24* (11), 5937–5954. https://doi.org/10.1111/jcmm.15180.

(3) Daiber, A.; Hahad, O.; Andreadou, I.; Steven, S.; Daub, S.; Münzel, T. Redox-Related Biomarkers in Human Cardiovascular Disease - Classical Footprints and Beyond. *Redox Biol* **2021**, *42*, 101875. https://doi.org/10.1016/j.redox.2021.101875.

(4) Heusch, G. Myocardial Ischaemia-Reperfusion Injury and Cardioprotection in Perspective. *Nat Rev Cardiol* **2020**, *17* (12), 773–789. https://doi.org/10.1038/s41569-020-0403-y.

(5) Gibbons, R. J.; Valeti, U. S.; Araoz, P. A.; Jaffe, A. S. The Quantification of Infarct Size. *J Am Coll Cardiol* **2004**, *44* (8), 1533–1542. https://doi.org/10.1016/j.jacc.2004.06.071.

(6) Heusch, G. Molecular Basis of Cardioprotection. *Circulation Research* **2015**, *116* (4), 674–699. https://doi.org/10.1161/CIRCRESAHA.116.305348.

(7) Lougiakis, N.; Papapetropoulos, A.; Gikas, E.; Toumpas, S.; Efentakis, P.; Wedmann, R.; Zoga, A.; Zhou, Z.; Iliodromitis, E. K.; Skaltsounis, A.-L.; Filipovic, M. R.; Pouli, N.; Marakos, P.; Andreadou, I. Synthesis and Pharmacological Evaluation of Novel Adenine–Hydrogen Sulfide Slow Release Hybrids Designed as Multitarget

Cardioprotective Agents. *Journal of Medicinal Chemistry* **2016**, *59* (5), 1776–1790. https://doi.org/10.1021/acs.jmedchem.5b01223.
(8) Lecour, S.; Andreadou, I.; Bøtker, H. E.; Davidson, S. M.; Heusch, G.; Ruiz-Meana, M.; Schulz, R.; Zuurbier, C. J.; Ferdinandy, P.; Hausenloy, D. J.; the European Union-CARDIOPROTECTION COST ACTION CA16225. IMproving Preclinical Assessment of Cardioprotective Therapies (IMPACT) Criteria: Guidelines of the EU-CARDIOPROTECTION COST Action. *Basic Res Cardiol* **2021**, *116* (1), 52. https://doi.org/10.1007/s00395-021-00893-5.
(9) Eltzschig, H. K.; Eckle, T. Ischemia and Reperfusion--from Mechanism to Translation. *Nat. Med.* **2011**, *17* (11), 1391–1401. https://doi.org/10.1038/nm.2507.
(10) Nikolaou, P.-E.; Boengler, K.; Efentakis, P.; Vouvogiannopoulou, K.; Zoga, A.; Gaboriaud-Kolar, N.; Myrianthopoulos, V.; Alexakos, P.; Kostomitsopoulos, N.; Rerras, I.; Tsantili-Kakoulidou, A.; Skaltsounis, A. L.; Papapetropoulos, A.; Iliodromitis, E. K.; Schulz, R.; Andreadou, I. Investigating and Re-Evaluating the Role of Glycogen Synthase Kinase 3 Beta Kinase as a Molecular Target for Cardioprotection by Using Novel Pharmacological Inhibitors. *Cardiovasc. Res.* **2019**, *115* (7), 1228–1243. https://doi.org/10.1093/cvr/cvz061.
(11) Nesci, S.; Trombetti, F.; Algieri, C.; Pagliarani, A. A Therapeutic Role for the F1FO-ATP Synthase. *SLAS Discov* **2019**, *24* (9), 893–903. https://doi.org/10.1177/2472555219860448.
(12) Pinke, G.; Zhou, L.; Sazanov, L. A. Cryo-EM Structure of the Entire Mammalian F-Type ATP Synthase. *Nat Struct Mol Biol* **2020**, *27* (11), 1077–1085. https://doi.org/10.1038/s41594-020-0503-8.
(13) Patel, B. A.; D'Amico, T. L.; Blagg, B. S. J. Natural Products and Other Inhibitors of F1FO ATP Synthase. *European Journal of Medicinal Chemistry* **2020**, *207*, 112779. https://doi.org/10.1016/j.ejmech.2020.112779.
(14) Fillingame, R. H.; Jiang, W.; Dmitriev, O. Y. Coupling H(+) Transport to Rotary Catalysis in F-Type ATP Synthases: Structure and Organization of the Transmembrane Rotary Motor. *J. Exp. Biol.* **2000**, *203* (Pt 1), 9–17.
(15) Ahmad, Z.; Hassan, S. S.; Azim, S. A Therapeutic Connection between Dietary Phytochemicals and ATP Synthase. *Curr Med Chem* **2017**, *24* (35), 3894–3906. https://doi.org/10.2174/0929867324666170823125330.
(16) Symersky, J.; Osowski, D.; Walters, D. E.; Mueller, D. M. Oligomycin Frames a Common Drug-Binding Site in the ATP Synthase. *Proceedings of the National Academy of Sciences* **2012**, *109* (35), 13961–13965. https://doi.org/10.1073/pnas.1207912109.
(17) van Raaij, M. J.; Abrahams, J. P.; Leslie, A. G.; Walker, J. E. The Structure of Bovine F1-ATPase Complexed with the Antibiotic Inhibitor Aurovertin B. *Proc Natl Acad Sci U S A* **1996**, *93* (14), 6913–6917.
(18) Gledhill, J. R.; Montgomery, M. G.; Leslie, A. G. W.; Walker, J. E. Mechanism of Inhibition of Bovine F1-ATPase by Resveratrol and Related Polyphenols. *Proc Natl Acad Sci U S A* **2007**, *104* (34), 13632–13637. https://doi.org/10.1073/pnas.0706290104.
(19) Zheng, J.; Ramirez, V. D. Inhibition of Mitochondrial Proton F0F1-ATPase/ATP Synthase by Polyphenolic Phytochemicals. *Br J Pharmacol* **2000**, *130* (5), 1115–1123. https://doi.org/10.1038/sj.bjp.0703397.
(20) Vinogradov, A. D. Steady-State and Pre-Steady-State Kinetics of the Mitochondrial F(1)F(o) ATPase: Is ATP Synthase a Reversible Molecular Machine? *J Exp Biol* **2000**, *203* (Pt 1), 41–49. https://doi.org/10.1242/jeb.203.1.41.
(21) Ivanes, F.; Faccenda, D.; Gatliff, J.; Ahmed, A. A.; Cocco, S.; Cheng, C. H. K.; Allan, E.; Russell, C.; Duchen, M. R.; Campanella, M. The Compound BTB06584 Is an IF1-Dependent Selective Inhibitor of the Mitochondrial F1Fo-ATPase. *British Journal of Pharmacology* **2014**, *171* (18), 4193–4206. https://doi.org/10.1111/bph.12638.

(22) Atwal, K. S.; Wang, P.; Rogers, W. L.; Sleph, P.; Monshizadegan, H.; Ferrara, F. N.; Traeger, S.; Green, D. W.; Grover, G. J. Small Molecule Mitochondrial F1F0 ATPase Hydrolase Inhibitors as Cardioprotective Agents. Identification of 4-(N-Arylimidazole)-Substituted Benzopyran Derivatives as Selective Hydrolase Inhibitors. *J. Med. Chem.* **2004**, *47* (5), 1081–1084. https://doi.org/10.1021/jm030291x.

(23) Grover, G. J.; Malm, J. Pharmacological Profile of the Selective Mitochondrial F1F0 ATP Hydrolase Inhibitor BMS-199264 in Myocardial Ischemia. *Cardiovascular Therapeutics* **2008**, *26* (4), 287–296. https://doi.org/10.1111/j.1755-5922.2008.00065.x.

(24) Campanella, M.; Casswell, E.; Chong, S.; Farah, Z.; Wieckowski, M. R.; Abramov, A. Y.; Tinker, A.; Duchen, M. R. Regulation of Mitochondrial Structure and Function by the F1Fo-ATPase Inhibitor Protein, IF1. *Cell Metab.* **2008**, *8* (1), 13–25. https://doi.org/10.1016/j.cmet.2008.06.001.

(25) Bøtker, H. E.; Hausenloy, D.; Andreadou, I.; Antonucci, S.; Boengler, K.; Davidson, S. M.; Deshwal, S.; Devaux, Y.; Di Lisa, F.; Di Sante, M.; Efentakis, P.; Femminò, S.; García-Dorado, D.; Giricz, Z.; Ibanez, B.; Iliodromitis, E.; Kaludercic, N.; Kleinbongard, P.; Neuhäuser, M.; Ovize, M.; Pagliaro, P.; Rahbek-Schmidt, M.; Ruiz-Meana, M.; Schlüter, K.-D.; Schulz, R.; Skyschally, A.; Wilder, C.; Yellon, D. M.; Ferdinandy, P.; Heusch, G. Practical Guidelines for Rigor and Reproducibility in Preclinical and Clinical Studies on Cardioprotection. *Basic Res. Cardiol.* **2018**, *113* (5), 39. https://doi.org/10.1007/s00395-018-0696-8.

(26) Fantel, A.-M.; Myrianthopoulos, V.; Georgoulis, A.; Lougiakis, N.; Zantza, I.; Lamprinidis, G.; Augsburger, F.; Marakos, P.; Vorgias, C. E.; Szabo, C.; Pouli, N.; Papapetropoulos, A.; Mikros, E. Screening of Heteroaromatic Scaffolds against Cystathionine Beta-Synthase Enables Identification of Substituted Pyrazolo[3,4-c]Pyridines as Potent and Selective Orthosteric Inhibitors. *Molecules* **2020**, *25* (16), 3739. https://doi.org/10.3390/molecules25163739.

(27) Myrianthopoulos, V.; Lambrinidis, G.; Mikros, E. In Silico Screening of Compound Libraries Using a Consensus of Orthogonal Methodologies. *Methods Mol Biol* **2018**, *1824*, 261–277. https://doi.org/10.1007/978-1-4939-8630-9_15.

(28) Okamoto, Y.; Ojika, M.; Suzuki, S.; Murakami, M.; Sakagami, Y. Iantherans A and B, Unique Dimeric Polybrominated Benzofurans as Na,K-ATPase Inhibitors from a Marine Sponge, Ianthella Sp. *Bioorganic & Medicinal Chemistry* **2001**, *9* (1), 179–183. https://doi.org/10.1016/S0968-0896(00)00234-0.

(29) Maurady, A.; M'guil, M.; Sadoq, B.-E.; Eslami, G.; Britel, M. R. Molecular Docking Study of Selected Molecules as Novel Targets for ATPase of Mycobacterium Tuberculosis Inhibitors. In *Advanced Intelligent Systems for Sustainable Development (AI2SD'2020)*; Kacprzyk, J., Balas, V. E., Ezziyyani, M., Eds.; Advances in Intelligent Systems and Computing; Springer International Publishing: Cham, 2022; pp 157–170. https://doi.org/10.1007/978-3-030-90633-7_15.

(30) Narang, R.; Kumar, R.; Kalra, S.; Nayak, S. K.; Khatik, G. L.; Kumar, G. N.; Sudhakar, K.; Singh, S. K. Recent Advancements in Mechanistic Studies and Structure Activity Relationship of FoF1 ATP Synthase Inhibitor as Antimicrobial Agent. *European Journal of Medicinal Chemistry* **2019**, *182*, 111644. https://doi.org/10.1016/j.ejmech.2019.111644.

(31) Acin-Perez, R.; Benincá, C.; Fernandez Del Rio, L.; Shu, C.; Baghdasarian, S.; Zanette, V.; Gerle, C.; Jiko, C.; Khairallah, R.; Khan, S.; Rincon Fernandez Pacheco, D.; Shabane, B.; Erion, K.; Masand, R.; Dugar, S.; Ghenoiu, C.; Schreiner, G.; Stiles, L.; Liesa, M.; Shirihai, O. S. Inhibition of ATP Synthase Reverse Activity Restores Energy Homeostasis in Mitochondrial Pathologies. *EMBO J* **2023**, *42* (10), e111699. https://doi.org/10.15252/embj.2022111699.

(32) Bernardi, P.; Rasola, A.; Forte, M.; Lippe, G. The Mitochondrial Permeability Transition Pore: Channel Formation by F-ATP Synthase, Integration in Signal Transduction, and Role in Pathophysiology. *Physiological Reviews* **2015**, *95* (4), 1111–1155. https://doi.org/10.1152/physrev.00001.2015.

(33) Amodeo, G. F.; Mnatsakanyan, N.; Solesio, M. E.; Klim, M.; Kurcok, P.; Zakharian, E.; Jonas, E. A.; Pavlov, E. V. Molecular Assembly of the Mitochondrial Permeability Transition Pore. *Biophysical Journal* **2018**, *114* (3), 658a. https://doi.org/10.1016/j.bpj.2017.11.3554.

(34) Boengler, K.; Hilfiker-Kleiner, D.; Heusch, G.; Schulz, R. Inhibition of Permeability Transition Pore Opening by Mitochondrial STAT3 and Its Role in Myocardial Ischemia/Reperfusion. *Basic Res Cardiol* **2010**, *105* (6), 771–785. https://doi.org/10.1007/s00395-010-0124-1.

(35) Giorgio, V.; Stockum, S. von; Antoniel, M.; Fabbro, A.; Fogolari, F.; Forte, M.; Glick, G. D.; Petronilli, V.; Zoratti, M.; Szabó, I.; Lippe, G.; Bernardi, P. Dimers of Mitochondrial ATP Synthase Form the Permeability Transition Pore. *PNAS* **2013**, *110* (15), 5887–5892. https://doi.org/10.1073/pnas.1217823110.

(36) Alavian, K. N.; Beutner, G.; Lazrove, E.; Sacchetti, S.; Park, H.-A.; Licznerski, P.; Li, H.; Nabili, P.; Hockensmith, K.; Graham, M.; Porter, G. A.; Jonas, E. A. An Uncoupling Channel within the C-Subunit Ring of the F1FO ATP Synthase Is the Mitochondrial Permeability Transition Pore. *Proceedings of the National Academy of Sciences* **2014**, *111* (29), 10580–10585. https://doi.org/10.1073/pnas.1401591111.

(37) Pagliarani, A.; Nesci, S.; Ventrella, V. Novel Drugs Targeting the C-Ring of the F1FO-ATP Synthase. *Mini Rev Med Chem* **2016**, *16* (10), 815–824. https://doi.org/10.2174/1389557516666160211120955.

(38) Mnatsakanyan, N.; Llaguno, M. C.; Yang, Y.; Yan, Y.; Weber, J.; Sigworth, F. J.; Jonas, E. A. A Mitochondrial Megachannel Resides in Monomeric F1FO ATP Synthase. *Nat Commun* **2019**, *10*. https://doi.org/10.1038/s41467-019-13766-2.

(39) Morciano, G.; Preti, D.; Pedriali, G.; Aquila, G.; Missiroli, S.; Fantinati, A.; Caroccia, N.; Pacifico, S.; Bonora, M.; Talarico, A.; Morganti, C.; Rizzo, P.; Ferrari, R.; Wieckowski, M. R.; Campo, G.; Giorgi, C.; Trapella, C.; Pinton, P. Discovery of Novel 1,3,8-Triazaspiro[4.5]Decane Derivatives That Target the c Subunit of F1/FO-Adenosine Triphosphate (ATP) Synthase for the Treatment of Reperfusion Damage in Myocardial Infarction. *Journal of Medicinal Chemistry* **2018**. https://doi.org/10.1021/acs.jmedchem.8b00278.

(40) Bernardi, P.; Gerle, C.; Halestrap, A. P.; Jonas, E. A.; Karch, J.; Mnatsakanyan, N.; Pavlov, E.; Sheu, S.-S.; Soukas, A. A. Identity, Structure, and Function of the Mitochondrial Permeability Transition Pore: Controversies, Consensus, Recent Advances, and Future Directions. *Cell Death Differ* **2023**, *30* (8), 1869–1885. https://doi.org/10.1038/s41418-023-01187-0.

(41) Castellano, S.; Taliani, S.; Viviano, M.; Milite, C.; Da Pozzo, E.; Costa, B.; Barresi, E.; Bruno, A.; Cosconati, S.; Marinelli, L.; Greco, G.; Novellino, E.; Sbardella, G.; Da Settimo, F.; Martini, C. Structure-Activity Relationship Refinement and Further Assessment of 4-Phenylquinazoline-2-Carboxamide Translocator Protein Ligands as Antiproliferative Agents in Human Glioblastoma Tumors. *J Med Chem* **2014**, *57* (6), 2413–2428. https://doi.org/10.1021/jm401721h.

(42) Siméon, F. G.; Lee, J.-H.; Morse, C. L.; Stukes, I.; Zoghbi, S. S.; Manly, L. S.; Liow, J.-S.; Gladding, R. L.; Dick, R. M.; Yan, X.; Taliani, S.; Costa, B.; Martini, C.; Da Settimo, F.; Castellano, S.; Innis, R. B.; Pike, V. W. Synthesis and Screening in Mice of Fluorine-Containing PET Radioligands for TSPO: Discovery of a Promising 18F-Labeled Ligand. *J. Med. Chem.* **2021**, *64* (22), 16731–16745. https://doi.org/10.1021/acs.jmedchem.1c01562.

(43) Michailidou, M.; Giannouli, V.; Kotsikoris, V.; Papadodima, O.; Kontogianni, G.; Kostakis, I. K.; Lougiakis, N.; Chatziioannou, A.; Kolisis, F. N.; Marakos, P.; Pouli, N.; Loutrari, H. Novel Pyrazolopyridine Derivatives as Potential Angiogenesis Inhibitors: Synthesis, Biological Evaluation and Transcriptome-Based Mechanistic Analysis. *Eur J Med Chem* **2016**, *121*, 143–157. https://doi.org/10.1016/j.ejmech.2016.05.035.

(44) Papastathopoulos, A.; Lougiakis, N.; Kostakis, I. K.; Marakos, P.; Pouli, N.; Pratsinis, H.; Kletsas, D. New Bioactive 5-Arylcarboximidamidopyrazolo[3,4-c]Pyridines: Synthesis, Cytotoxic Activity, Mechanistic Investigation and Structure-Activity Relationships. *Eur J Med Chem* **2021**, *218*, 113387. https://doi.org/10.1016/j.ejmech.2021.113387.

(45) Tangallapally, R. P.; Yendapally, R.; Lee, R. E.; Lenaerts, A. J. M.; Lee, R. E. Synthesis and Evaluation of Cyclic Secondary Amine Substituted Phenyl and Benzyl Nitrofuranyl Amides as Novel Antituberculosis Agents. *J Med Chem* **2005**, *48* (26), 8261–8269. https://doi.org/10.1021/jm050765n.

(46) Baell, J. B.; Holloway, G. A. New Substructure Filters for Removal of Pan Assay Interference Compounds (PAINS) from Screening Libraries and for Their Exclusion in Bioassays. *J. Med. Chem.* **2010**, *53* (7), 2719–2740. https://doi.org/10.1021/jm901137j.

(47) Kobayashi, R.; Ueno, H.; Okazaki, K.; Noji, H. Molecular Mechanism on Forcible Ejection of ATPase Inhibitory Factor 1 from Mitochondrial ATP Synthase. *Nat Commun* **2023**, *14* (1), 1682. https://doi.org/10.1038/s41467-023-37182-9.

(48) Watanabe, R.; Noji, H. Chemomechanical Coupling Mechanism of F 1-ATPase: Catalysis and Torque Generation. *FEBS Letters* **2013**, *587* (8), 1030–1035. https://doi.org/10.1016/j.febslet.2013.01.063.

(49) Jennings, R. B.; Reimer, K. A.; Steenbergen, C. Effect of Inhibition of the Mitochondrial ATPase on Net Myocardial ATP in Total Ischemia. *Journal of Molecular and Cellular Cardiology* **1991**, *23* (12), 1383–1395. https://doi.org/10.1016/0022-2828(91)90185-O.

(50) Davidson, S. M.; Ferdinandy, P.; Andreadou, I.; Bøtker, H. E.; Heusch, G.; Ibáñez, B.; Ovize, M.; Schulz, R.; Yellon, D. M.; Hausenloy, D. J.; Garcia-Dorado, D.; Action (CA16225), on behalf of the E. U. C. C. Multitarget Strategies to Reduce Myocardial Ischemia/Reperfusion Injury: JACC Review Topic of the Week. *Journal of the American College of Cardiology* **2019**, *73* (1), 89–99. https://doi.org/10.1016/j.jacc.2018.09.086.

(51) Wu, J.-W.; Hu, H.; Hua, J.; Ma, L.-K. ATPase Inhibitory Factor 1 Protects the Heart from Acute Myocardial Ischemia/Reperfusion Injury through Activating AMPK Signaling Pathway. *International Journal of Biological Sciences* **2022**, *18* (2), 731–741. https://doi.org/10.7150/ijbs.64956.

(52) Nikolaou, P. E.; Efentakis, P.; Abu Qourah, F.; Femminò, S.; Makridakis, M.; Kanaki, Z.; Varela, A.; Tsoumani, M.; Davos, C. H.; Dimitriou, C. A.; Tasouli, A.; Dimitriadis, G.; Kostomitsopoulos, N.; Zuurbier, C. J.; Vlahou, A.; Klinakis, A.; Brizzi, M. F.; Iliodromitis, E. K.; Andreadou, I. Chronic Empagliflozin Treatment Reduces Myocardial Infarct Size in Nondiabetic Mice Through STAT-3-Mediated Protection on Microvascular Endothelial Cells and Reduction of Oxidative Stress. *Antioxid Redox Signal* **2021**, *34* (7), 551–571. https://doi.org/10.1089/ars.2019.7923.

(53) Garcia, N. A.; Moncayo-Arlandi, J.; Vazquez, A.; Genovés, P.; Calvo, C. J.; Millet, J.; Martí, N.; Aguado, C.; Knecht, E.; Valiente-Alandi, I.; Montero, J. A.; Díez-Juan, A.; Sepúlveda, P. Hydrogen Sulfide Improves Cardiomyocyte Function in a Cardiac Arrest Model. *Ann Transplant* **2017**, *22*, 285–295. https://doi.org/10.12659/aot.901410.

(54) Musters, R. J.; Pröbstl-Biegelmann, E.; van Veen, T. A.; Hoebe, K. H.; Op den Kamp, J. A.; Verkleij, A. J.; Post, J. A. Sarcolemmal Phosphatidylethanolamine Reorganization during Simulated Ischaemia and Reperfusion: Reversibility and ATP Dependency. *Mol Membr Biol* **1996**, *13* (3), 159–164. https://doi.org/10.3109/09687689609160592.

(55) Woo, S.-H.; Trinh, T. N. P2 Receptors in Cardiac Myocyte Pathophysiology and Mechanotransduction. *Int J Mol Sci* **2020**, *22* (1), 251. https://doi.org/10.3390/ijms22010251.
(56) von Kügelgen, I. Pharmacological Profiles of Cloned Mammalian P2Y-Receptor Subtypes. *Pharmacol Ther* **2006**, *110* (3), 415–432. https://doi.org/10.1016/j.pharmthera.2005.08.014.
(57) Djerada, Z.; Feliu, C.; Richard, V.; Millart, H. Current Knowledge on the Role of P2Y Receptors in Cardioprotection against Ischemia-Reperfusion. *Pharmacol Res* **2017**, *118*, 5–18. https://doi.org/10.1016/j.phrs.2016.08.009.
(58) Tong, H.; Bernstein, D.; Murphy, E.; Steenbergen, C. The Role of β-Adrenergic Receptor Signaling in Cardioprotection. *The FASEB Journal* **2005**, *19* (8), 983–985. https://doi.org/10.1096/fj.04-3067fje.
(59) Masterson, L. R.; Yu, T.; Shi, L.; Wang, Y.; Gustavsson, M.; Mueller, M. M.; Veglia, G. cAMP-Dependent Protein Kinase A Selects the Excited State of the Membrane Substrate Phospholamban. *J Mol Biol* **2011**, *412* (2), 155–164. https://doi.org/10.1016/j.jmb.2011.06.041.
(60) Bibli, S.-I.; Andreadou, I.; Chatzianastasiou, A.; Tzimas, C.; Sanoudou, D.; Kranias, E.; Brouckaert, P.; Coletta, C.; Szabo, C.; Kremastinos, D. T.; Iliodromitis, E. K.; Papapetropoulos, A. Cardioprotection by H2S Engages a cGMP-Dependent Protein Kinase G/Phospholamban Pathway. *Cardiovasc Res* **2015**, *106* (3), 432–442. https://doi.org/10.1093/cvr/cvv129.
(61) Haghighi, K.; Bidwell, P.; Kranias, E. G. Phospholamban Interactome in Cardiac Contractility and Survival: A New Vision of an OLD Friend. *J Mol Cell Cardiol* **2014**, *0*, 160–167. https://doi.org/10.1016/j.yjmcc.2014.10.005.
(62) Giorgi, C.; Baldassari, F.; Bononi, A.; Bonora, M.; De Marchi, E.; Marchi, S.; Missiroli, S.; Patergnani, S.; Rimessi, A.; Suski, J. M.; Wieckowski, M. R.; Pinton, P. Mitochondrial Ca2+ and Apoptosis. *Cell Calcium* **2012**, *52* (1), 36–43. https://doi.org/10.1016/j.ceca.2012.02.008.
(63) Manni, S.; Mauban, J. H.; Ward, C. W.; Bond, M. Phosphorylation of the cAMP-Dependent Protein Kinase (PKA) Regulatory Subunit Modulates PKA-AKAP Interaction, Substrate Phosphorylation, and Calcium Signaling in Cardiac Cells*. *Journal of Biological Chemistry* **2008**, *283* (35), 24145–24154. https://doi.org/10.1074/jbc.M802278200.
(64) Katrukha, I. A.; Katrukha, A. G. Myocardial Injury and the Release of Troponins I and T in the Blood of Patients. *Clinical Chemistry* **2021**, *67* (1), 124–130. https://doi.org/10.1093/clinchem/hvaa281.
(65) Rossello, X.; Yellon, D. M. The RISK Pathway and Beyond. *Basic Res Cardiol* **2018**, *113* (1). https://doi.org/10.1007/s00395-017-0662-x.
(66) Hausenloy, D. J.; Yellon, D. M. Reperfusion Injury Salvage Kinase Signalling: Taking a RISK for Cardioprotection. *Heart Fail Rev* **2007**, *12* (3–4), 217–234. https://doi.org/10.1007/s10741-007-9026-1.
(67) Hausenloy, D. J.; Yellon, D. M. Ischaemic Conditioning and Reperfusion Injury. *Nature Reviews Cardiology* **2016**, *13* (4), 193–209. https://doi.org/10.1038/nrcardio.2016.5.
(68) Senoo, H.; Murata, D.; Wai, M.; Arai, K.; Iwata, W.; Sesaki, H.; Iijima, M. KARATE: PKA-Induced KRAS4B-RHOA-mTORC2 Supercomplex Phosphorylates AKT in Insulin Signaling and Glucose Homeostasis. *Mol Cell* **2021**, *81* (22), 4622-4634.e8. https://doi.org/10.1016/j.molcel.2021.09.001.
(69) Bellis, A.; Castaldo, D.; Trimarco, V.; Monti, M. G.; Chivasso, P.; Sadoshima, J.; Trimarco, B.; Morisco, C. Cross-Talk between PKA and Akt Protects Endothelial Cells from Apoptosis in the Late Ischemic Preconditioning. *Arterioscler Thromb Vasc Biol* **2009**, *29* (8), 1207–1212. https://doi.org/10.1161/ATVBAHA.109.184135.

(70) García-Morales, V.; Luaces-Regueira, M.; Campos-Toimil, M. The cAMP Effectors PKA and Epac Activate Endothelial NO Synthase through PI3K/Akt Pathway in Human Endothelial Cells. *Biochem Pharmacol* **2017**, *145*, 94–101. https://doi.org/10.1016/j.bcp.2017.09.004.
(71) Wu, M.-Y.; Yiang, G.-T.; Liao, W.-T.; Tsai, A. P.-Y.; Cheng, Y.-L.; Cheng, P.-W.; Li, C.-Y.; Li, C.-J. Current Mechanistic Concepts in Ischemia and Reperfusion Injury. *Cell. Physiol. Biochem.* **2018**, *46* (4), 1650–1667. https://doi.org/10.1159/000489241.
(72) Davidson, S. M.; Adameová, A.; Barile, L.; Cabrera-Fuentes, H. A.; Lazou, A.; Pagliaro, P.; Stensløkken, K.; Garcia-Dorado, D. Mitochondrial and Mitochondrial-independent Pathways of Myocardial Cell Death during Ischaemia and Reperfusion Injury. *J Cell Mol Med* **2020**, *24* (7), 3795–3806. https://doi.org/10.1111/jcmm.15127.
(73) Del Re, D. P.; Amgalan, D.; Linkermann, A.; Liu, Q.; Kitsis, R. N. Fundamental Mechanisms of Regulated Cell Death and Implications for Heart Disease. *Physiol Rev* **2019**, *99* (4), 1765–1817. https://doi.org/10.1152/physrev.00022.2018.
(74) Namura, S.; Zhu, J.; Fink, K.; Endres, M.; Srinivasan, A.; Tomaselli, K. J.; Yuan, J.; Moskowitz, M. A. Activation and Cleavage of Caspase-3 in Apoptosis Induced by Experimental Cerebral Ischemia. *J Neurosci* **1998**, *18* (10), 3659–3668. https://doi.org/10.1523/JNEUROSCI.18-10-03659.1998.
(75) Hunzicker-Dunn, M. E.; Lopez-Biladeau, B.; Law, N. C.; Fiedler, S. E.; Carr, D. W.; Maizels, E. T. PKA and GAB2 Play Central Roles in the FSH Signaling Pathway to PI3K and AKT in Ovarian Granulosa Cells. *Proceedings of the National Academy of Sciences* **2012**, *109* (44), E2979–E2988. https://doi.org/10.1073/pnas.1205661109.
(76) Chinnadurai, G.; Vijayalingam, S.; Gibson, S. B. BNIP3 Subfamily BH3-Only Proteins: Mitochondrial Stress Sensors in Normal and Pathological Functions. *Oncogene* **2008**, *27* (1), S114–S127. https://doi.org/10.1038/onc.2009.49.
(77) Hawkins, P. C. D.; Skillman, A. G.; Warren, G. L.; Ellingson, B. A.; Stahl, M. T. Conformer Generation with OMEGA: Algorithm and Validation Using High Quality Structures from the Protein Databank and Cambridge Structural Database. *J. Chem. Inf. Model.* **2010**, *50* (4), 572–584. https://doi.org/10.1021/ci100031x.
(78) Hawkins, P. C. D.; Skillman, A. G.; Nicholls, A. Comparison of Shape-Matching and Docking as Virtual Screening Tools. *J. Med. Chem.* **2007**, *50* (1), 74–82. https://doi.org/10.1021/jm0603365.
(79) Andreadou, I.; Efentakis, P.; Balafas, E.; Togliatto, G.; Davos, C. H.; Varela, A.; Dimitriou, C. A.; Nikolaou, P.-E.; Maratou, E.; Lambadiari, V.; Ikonomidis, I.; Kostomitsopoulos, N.; Brizzi, M. F.; Dimitriadis, G.; Iliodromitis, E. K. Empagliflozin Limits Myocardial Infarction in Vivo and Cell Death in Vitro: Role of STAT3, Mitochondria, and Redox Aspects. *Frontiers in Physiology* **2017**, *8*. https://doi.org/10.3389/fphys.2017.01077.
(80) Plamiera; Carlos M.; Rolo; Anabela P. *Mitochondrial Regulation Methods and Protocols*; Methods in Molecular Biology; Humana Press, 2015; Vol. 1241.
(81) Zhou, A.; Rohou, A.; Schep, D. G.; Bason, J. V.; Montgomery, M. G.; Walker, J. E.; Grigorieff, N.; Rubinstein, J. L. Structure and Conformational States of the Bovine Mitochondrial ATP Synthase by Cryo-EM. *eLife* **2015**, *4*, e10180. https://doi.org/10.7554/eLife.10180.
(82) Watt, I. N.; Montgomery, M. G.; Runswick, M. J.; Leslie, A. G. W.; Walker, J. E. Bioenergetic Cost of Making an Adenosine Triphosphate Molecule in Animal Mitochondria. *Proceedings of the National Academy of Sciences* **2010**, *107* (39), 16823–16827. https://doi.org/10.1073/pnas.1011099107.
(83) Nikolaou, P. E.; Mylonas, N.; Makridakis, M.; Makrecka-Kuka, M.; Iliou, A.; Zerikiotis, S.; Efentakis, P.; Kampoukos, S.; Kostomitsopoulos, N.; Vilskersts, R.; Ikonomidis, I.; Lambadiari, V.; Zuurbier, C. J.; Latosinska, A.; Vlahou, A.; Dimitriadis, G.; Iliodromitis, E. K.; Andreadou, I. Cardioprotection by Selective SGLT-2 Inhibitors in a Non-Diabetic

1 Mouse Model of Myocardial Ischemia/Reperfusion Injury: A Class or a Drug Effect?
2 *Basic Res Cardiol* **2022**, *117* (1), 27. https://doi.org/10.1007/s00395-022-00934-7.
3

Table Of Contents Graphic